# RF MEMS Switches: Survey and Analysis

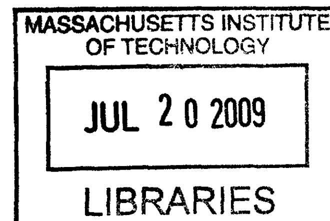
MASSACHUSETTS INSTITUTE OF TECHNOLOGY
JUL 20 2009
LIBRARIES

by

Antoinne Y. Machal-Cajigas

Submitted to the Department of Electrical Engineering and Computer Science

in partial fulfillment of the requirements for the degree of

Master of Engineering in Electrical Engineering and Computer Science

at the

MASSACHUSETTS INSTITUTE OF TECHNOLOGY

ARCHIVES

June 2009

© Antoinne Y. Machal-Cajigas, MMIX. All rights reserved.

The author hereby grants to MIT permission to reproduce and distribute publicly paper and electronic copies of this thesis document in whole or in part.

Author . . . . . . . . . . . . . . . . . . . . . . . . . . . . . . . . . . . . . . . . . . . .
Department of Electrical Engineering and Computer Science
May 21, 2009

Certified by. . . . . . . . . . . . . . . . . . . . . . . . . . . . . . . . . . . . . . . . . . . .
Jeffrey H. Lang
Professor of Electrical Engineering
Department of Electrical Engineering & Computer Science
M.I.T. Thesis Supervisor

Certified by. . . . . . . . . . . . . . . . . . . . . . . . . . . . . . . . . . . . . . . . . . . .
Bryan Johnson
Supply Base Management Manager
Teradyne
VI-A Company Thesis Supervisor

Accepted by . . . . . . . . . . . . . . . . . . . . . . . . . . . . . . . . . . . . . . . . . . . .
Arthur C. Smith
Chairman, Department Committee on Graduate Students

# RF MEMS Switches: Survey and Analysis

by

Antoinne Y. Machal-Cajigas

Submitted to the Department of Electrical Engineering and Computer Science on May 22, 2009, in partial fulfillment of the requirements for the degree of Master of Engineering in Electrical Engineering and Computer Science

## Abstract

Microelectromechanical systems known as MEMS, are an enabling technology that describe a field capable of creating very small electromechanical devices with feature sizes on the order of microns, or $10^{-6}$ meters. MEMS technology has received considerable attention recently as a way to produce switches. The technology leverages the fabrication instruments, processing and design techniques of the mature integrated circuit (IC) industry. While MEMS technology has shown great successes in producing commercial devices like accelerometers and pressure sensors, the same has not been true for switches. MEMS switches have shown great RF characteristics via low losses and high isolation. However, they possess several important shortcomings. At present, RF MEMS switches have low reliability, limited power handling capabilities, and slow switching times. Nonetheless, MEMS switches are poised to provide advantages over other switching technologies. The goal of this thesis is to understand the limits of their operation and predict their impact in practical applications. To that end, this thesis surveys the present state of the art of MEMS RF switches, identifies the benefits and drawbacks of switches created using this technology, and formulates predictions for the future of MEMS RF switches.

Thesis Supervisor: Jeffrey H. Lang
Title: Professor, Department of Electrical Engineering and Computer Science

# Acknowledgements

I want to take a moment to thank the many individuals who helped make this work a reality.

To my MIT advisor Professor Lang for providing me a medium in which to discuss the science of my thesis and his willingness to help me on what often seemed like short notice. He has been a wonderful advisor whose guidance has been priceless.

To my Teradyne advisor Bryan Johnson who first presented RF MEMS switches as an interesting project. His comments have helped me put the science of RF MEMS switches into perspective with the larger issue of switching technology.

To Antonio Pina, Tom Gannon, Bryan Hynes, and Dan Weisen for extending their help in gathering and analyzing information pertaining to switches.

And last, but not least, to my parents and sister – Jorge, Helen and Jeda – who have supported me from the start.

# Contents


Chapter 1 ..... 15
Chapter 2 ..... 17
2.1 Switch Types ..... 17
2.1.1 Capacitive Switch ..... 17
Figure 2-1. Schematic of MEMS switch ..... 18
2.1.2 Ohmic Switch ..... 18
Figure 2-2. Schematic of MEMS relay ..... 19
2.2 Use at Radio Frequency ..... 19
2.3 Reliability ..... 20
2.3.1 Contact Resistance ..... 20
2.3.2 Stiction ..... 21
2.4 Typical Characteristics ..... 22
Chapter 3 ..... 23
3.1 Fixed-Fixed Structure (Capacitive switch) ..... 24
3.2 Fixed-Free Structure (Ohmic switch) ..... 25
3. 3 Switching Speed ..... 26
Chapter 4 ..... 28
4.1 Capacitive Switch ..... 28
4.2 Ohmic Switch ..... 28
4.3 Parasitics ..... 29
4.3.1 Capacitive Switch ..... 29
4.3.2 Ohmic Switch ..... 30
4.4 Transmission lines ..... 31
4.4.1 Extent of effects ..... 32
4.4.2 Microstrip Transmission Line ..... 34
4.4.3 Coplanar Wave Guides ..... 38
4.4.4 Synthesis ..... 40
4.5 Actuation Voltage ..... 41
4.5.1 Conventional first order model ..... 41

4.5.2 Refined Model ........ 43
4.5.3 Other considerations ........ 44
4.6 S-parameters ........ 44
4.7 Complete Device Model ........ 45
4.7.1 Ohmic Switch ........ 45
4.7.2 Capacitive Switch ........ 46
4.7.3 ABCD Matrix and Losses ........ 47
Chapter 5 ........ 48
5.1 Contact Resistance ........ 48
5.2 Stiction ........ 54
5.3 Switch Designs ........ 55
5.4 System Integration ........ 56
5.5 New Materials ........ 57
5.6 Fabrication Techniques ........ 57
5.7 Reliability ........ 63
Chapter 6 ........ 64
6.1 Down state Capacitance ........ 64
6.1.1 Thickness of Insulating Layer ........ 65
6.2 Up State Capacitance ........ 65
6.3 Incorporating the Actuation Voltage ........ 67
6.4 Attenuation ........ 69
6.5 Losses ........ 72
6.5.1 Insertion Loss ........ 72
6.5.2 Return Loss ........ 73
6.5.3 Isolation Loss ........ 74
6.6 Comparison ........ 76
Chapter 7 ........ 80
7.1 Packaging Methods ........ 80
7.2 Packaging Materials ........ 82
7.3 Die Placement in Package ........ 82
7.4 Wire Bonding and Sealing ........ 83
7.5 Bonding Technologies ........ 84
7.6 Standards ........ 85
7.7 Operational Environment ........ 86

7.8 Wafer Level Packaging ... 86
Chapter 8 ... 87
8.1 Summary ... 87
8.2 Conclusion ... 88
Chapter 9 ... 89
9.1 Insertion Loss ... 89
9.2 Return Loss ... 91
9.3 Isolation Loss ... 93
Bibliography ... 95

# List of Figures

**Figure 2-1.** Schematic of MEMS switch ........ 18
**Figure 2-2.** Schematic of MEMS relay ........ 19
**Figure 2-3.** Contact resistance over time ........ 21
**Figure 3-1.** Structural model of the fixed-fixed beam at rest and when actuated ........ 24
**Figure 3-2.** Fixed-Free beam subject to a partially distributed load ........ 26
**Figure 4-1.** Conventional on state and off state impedance model of the capacitive shunt MEMS switch ........ 28
**Figure 4-2.** Conventional off state and on state series impedance model of the ohmic contact MEMS series switches ........ 29
**Figure 4-3.** Basic layout of the capacitive MEMS shunt switch ........ 30
**Figure 4-4.** Parasitics for the (a) up and (b) down state of the ohmic switch ........ 30
**Figure 4-5.** Typical time domain picosecond pulse propagation ........ 32
**Figure 4-6.** Effective permittivity and attenuation for a CPW line on GaAs substrate .. 33
**Figure 4-7.** Effective dielectric constant versus width to height ratios with operation from DC to 50GHz. ........ 33
**Figure 4-8.** Microstrip configuration. ........ 34
**Figure 4-9.** CPW configuration ........ 38
**Figure 4-10.** Parallel plate capacitor model of an RF MEMS switch. ........ 41
**Figure 4-11.** Complete off state model of the ohmic switch ........ 45
**Figure 4-12.** Complete on state model of the ohmic switch ........ 46
**Figure 4-13.** Complete up state model of the capacitive switch ........ 46
**Figure 4-14.** Complete down state model of the capacitive switch ........ 46
**Figure 5-1.** Dual pulsed actuation waveform ........ 49
**Figure 5-2.** Decrease in contact resistance with temperature increase in chip substrate . 50
**Figure 5-3.** Contact asperities in contact surfaces ........ 51
**Figure 5-4.** 3D surface roughness created using fractal geometry ........ 52
**Figure 5-5.** Real contact area and number of contact spots as a function of time of device operation ........ 53
**Figure 5-6.** Dependence of resistance degradation on gap closure rate for an applied voltage of 3.3V ........ 54
**Figure 5-7.** Complex structures created using multidimensional UV exposure scheme. 59
**Figure 5-8.** Concentric cones created using multidimensional UV exposure scheme.... 61
**Figure 6-1.** Line attenuation versus line frequency for line dimensions of w, s and l equal to 100µm, 60µm, and 500µm respectively ........ 71
**Figure 6-2.** Insertion loss versus frequency for 5V, 10V, and 20V switch ........ 72
**Figure 6-3.** Return loss versus frequency for 5V, 10V, and 20V switch ........ 73
**Figure 6-4.** Isolation loss versus frequency for 5V, 10V, and 20V switch ........ 75
**Figure 7-1.** Illustration of (a) wafer bonding and (b) wafer level packaging ........ 82
**Figure 7-2.** Differences in electrical characteristics based on packaging modes ........ 86

# List of Tables

**Table 2-1.** Summary of important characteristics for different switch types .................. 20
**Table 2-2.** Typical values of characteristics for different switch technologies ................ 22
**Table 4-1.** Extent of errors in [3] ......................................................................... 44
**Table 6-1.** Dimensions for $SiO_2$ beam needed for particular actuation voltages ...... **Error! Bookmark not defined.**
**Table 6-2.** Down to up state capacitance ratio for each actuation design ....................... 68
**Table 6-3.** Variation of actuation voltage with a residual stress of 10MPa ..................... 69
**Table 6-4.** New dimensions using single crystal silicon ................................................ 69
**Table 6-5.** The attenuation in dB of the entire line as it varies with frequency and transmission line geometry ........................................................................................ 70
**Table 6-6.** Summary of results ................................................................................ 76
**Table 6-7.** Modified summary of important characteristics for different switch types... 78
**Table 6-8.** Comparison of the important characteristics for different switch types ........ 79

# Chapter 1

# Introduction

Microelectromechanical systems, otherwise known as MEMS, are an enabling technology that describe a field capable of creating very small devices with feature sizes on the order of microns, or $10^{-6}$ meters. The technology itself leverages off of the integrated circuit (IC) industry, using much of the same fabrication instruments, processing, and design techniques. MEMS technology creates moving devices on silicon substrates. One example of a MEMS device is a sensor. Sensors can measure flow, pressure, and even acceleration. Accelerometers have entered the commercial industry very successfully as produced by Analog Devices. MEMS technology has introduced the ability to make smaller versions of much larger systems.

MEMS technology has received a lot of attention recently as a way to produce switches. The first radio frequency (RF) MEMS switch was created in 1991 [1]. The first proof of concept design had excellent RF characteristics: low insertion and return loss, high isolation up to tens of gigahertz, in addition to drawing negligible power. Since then, special attention has been given to this class of switches, with research focused on increasing the upper bounds of these characteristics. These qualities make MEMS switches prime candidates to replace GaAs PIN diode switches, optoFETS and RF CMOS currently used in RF systems [2].

There are several designs for MEMS devices, and in particular for switches. In addition to including the traditional ohmic type switch, RF MEMS switches include shunt type capacitive switches, which rather than passing a signal, short the signal to ground. Moreover, there are numerous ways in which to actuate these switches, including electrostatics, comb drives or bimorph (using differences in thermal coefficients of expansions of materials); one can also combine these to create hybrid actuations.

Common applications of switches include signal routing, impedance matching networks, adjustable gain amplifiers, logic operation and telecommunications [3-4]. The simple function of both connecting and isolating input and output make the switch an extremely important component in the field of electronics. The needs for switches range across a broad spectrum. Depending on the design, switches must be small, cheap, fast actuating, reliable, capable of handling high power, or have very good high frequency characteristics. Due to the tradeoffs among these characteristics, no one switch can be used in all cases.

RF MEMS switches are no exception to this paradigm. While the field of switch technology is expected to benefit from the characteristics offered by MEMS technology, RF MEMS switches have several of shortcomings. RF MEMS switches are limited to much lower currents as compared to their solid-state counterparts. Due to mechanical actuation, RF MEMS switches are inherently slower than electronic switches [30]. RF MEMS cannot be used in telecommunication applications where switching speed is as important as the signals being switched. In addition, RF MEMS switches have low reliability. As an ohmic RF MEMS switch is actuated on and off, the resistance fluctuates over time and the contacts can stick together. This same effect takes a different form in capacitive switches: instead of contacts sticking together permanently, trapped charges in the dielectric layer keep the switch stuck in the down state even when no actuation signal is being applied. Although MEMS devices have enormous potential to provide advantages over existing technologies, the goal remains to thoroughly understand the boundaries of these benefits.

This thesis serves three purposes. The first is to survey the present state of the art device. The survey investigates RF MEMS switch developments both in the industry and the academic realm. The second is to understand the benefits and drawbacks of MEMS as a switching technology. Electrical characteristics of the RF MEMS switch such as pull-in voltage and RF losses will be analyzed. The mechanical behavior of the switch, namely dynamics will also be explored. The assessment of these characteristics of RF MEMS switches via models will highlight tradeoffs and potential limitations in creating a switch. The third is to formulate predictions about the future of MEMS technology.

# Chapter 2

# Background

A background in RF MEMS switches begin by addressing the two different types of designs and how they work, followed by a summary of how RF MEMS switches are used. Contact resistance and stiction will be addressed as factors that affect the reliability of MEMS devices. The tradeoffs in characteristics of these switches will be presented and related to reliability. Finally, typical characteristics of MEMS and different switching technology will be presented to facilitate in the comparison of the results of this survey.

## 2.1 Switch Types

There are two basic forms of a RF MEMS switch: an ohmic contact switch and a capacitive shunt switch. There are certainly other types of switch designs that exist, and even among these two there is a vast array of complicated design structures. The ohmic and capacitive type switches, however, represent the most commonly used. This survey will analyze these two forms.

### 2.1.1 Capacitive Switch

A MEMS switch involves a capacitance coupling contact consisting of a thin dielectric film and an air gap between two conductive, usually metallic, surfaces as shown in Figure 2-1. In capacitive switches (either capacitive membrane switches or capacitance shunt switches), the control voltage and the signal are superimposed and applied to the signal line. A dielectric film is deposited on the signal line, with an air gap separating the dielectric film and the suspended bridge grounded by anchors. In the up-state configuration displayed in Figure 2-1c the signal passes through the signal line because of the minimal capacitance coupling between the bottom signal line and the suspended bridge. When a switching control voltage is applied between the bridge and the bottom signal line, an electrostatic force is generated and pulls the bridge into contact with the dielectric film. This action produces a metal-insulator-metal contact interface shown in Figure 2-1d. Such a configuration increases the coupling capacitance between the signal line and the grounded bridge. The result is a small impedance at RF frequencies between the signal line and the ground that prevents the signal from passing through the output signal terminal. Thus, the air gap is electromechanically adjusted to achieve a capacitance change between the up-state and down-state configurations. A high down-to-up-state

capacitance ratio is of great importance for capacitive switches [28]. This ratio serves as a figure of merit to describe how well the switch operates as a true switch, which is completely off when open circuited and completely on when short circuited. These devices are designed for high frequency operation.

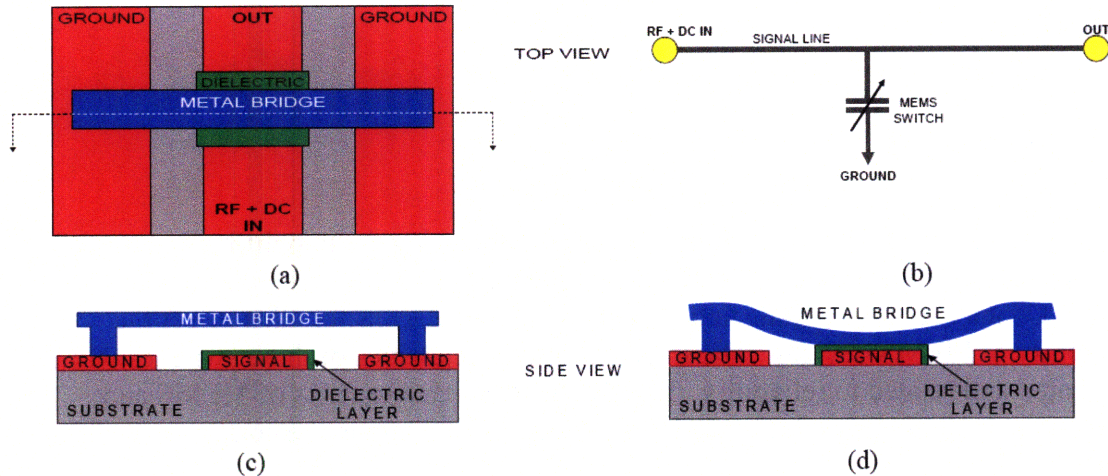


**Figure 2-1.** Schematic of MEMS switch: (a) top view, (b) equivalent electrical circuit, (c) up-state where current flows from in to out, and (d) down-state where current flows from in to ground.

### 2.1.2 Ohmic Switch

In contrast to a capacitive switch, an ohmic switch uses a metal-to-metal contact as displayed in Figure 2-2a. In ohmic switches, a cantilever deflects to close a gap in the signal line, which separates the input from the output signal terminals. This cantilever supports a metal contact bar and a drive metal plate. When a voltage is applied between the drive metal plate and the underlying electrode, an electrostatic force is produced to pull the contact bar toward the substrate. This causes the metal bar to bridge the gap in the signal line and electrically connect it to produce a metal-to-metal contact interface illustrated in Figure 2-2b. The absence of capacitive coupling along with the presence of this ohmic contact allows the cantilever relay to be used at both low and high frequencies. Although both metal contacting and capacitive coupling switches can be used as either a serial or shunt switch, metal contacting switches are usually used as serial switches, while capacitive coupling switches are commonly used for shunt switches [28].

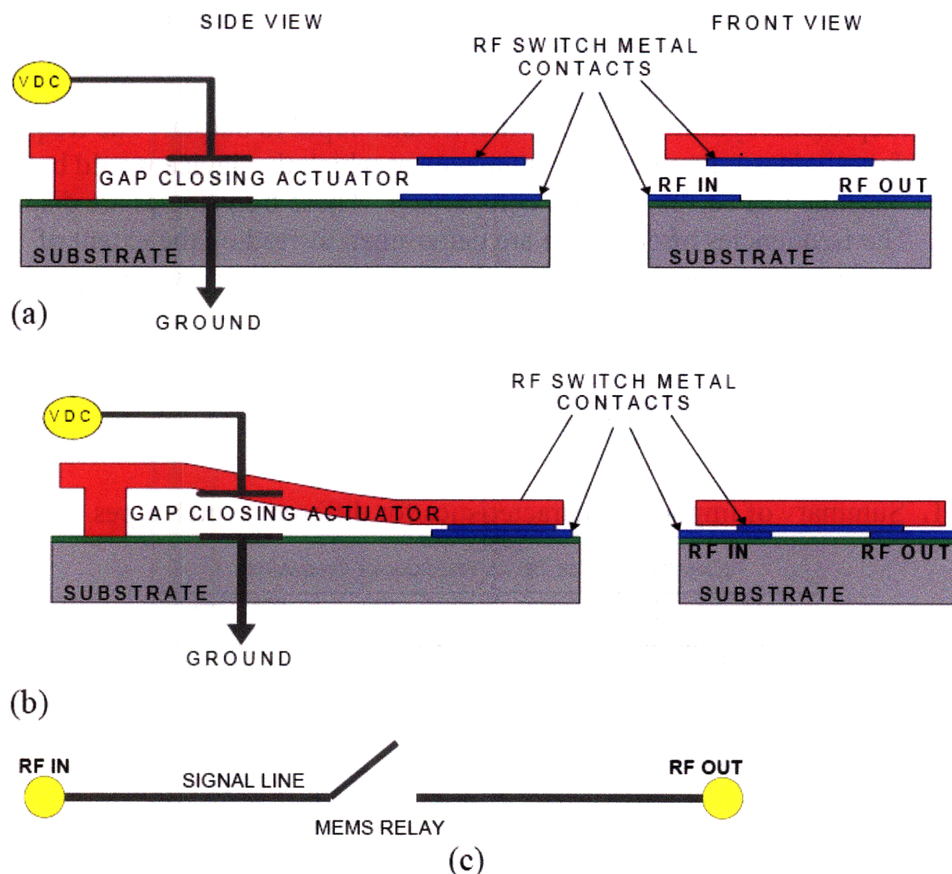


**Figure 2-2**. Schematic of MEMS relay: (a) up-state where current flow is inhibited between in and out, (b) down-state where current flows from in to out, and (c) equivalent electrical circuit.

## 2.2 Use at Radio Frequency

While RF MEMS switches can be cycled quickly, the term RF MEMS does not imply that a micromechanical system is actuating at RF frequencies [4]. In general, the micromechanical operation is used to actuate a separate RF device or component. RF MEMS refers almost entirely to the signal that is being stopped or passed through by the switch. In this work, RF MEMS refers to a switch that passes signals at RF frequencies. Later sections will discuss dynamic switching, where the switch is actuated on and off very quickly.

Between the two different types of switches, the capacitive switch is the best suited for RF switching applications. One of its advantages is that the insertion loss (attenuation from input to output) in the on state is independent of the contact force [2]. There are figures of merit to rate how good different switches are within these two domains. For shunt capacitive switches, the figure of merit is the ratio of the on state to the off state capacitance. This ratio describes how good a switch is at connecting input to output when on and isolating the two when off. A good switch of this form will have a very

high ratio. The figure of merit for an ohmic switch, on the other hand, is represented by a cutoff frequency of the form in equation (1) where $R_{on}$ is the on state resistance, representing how good the input connects to the output, and $C_{off}$ is the off state capacitance, representing how well the switch isolates input to output. The frequency of this figure of merit does not represent a frequency at which the device would be operated, but rather a baseline that serves only for comparison. These frequencies are displayed in Table 2-1. The frequencies of operation are determined instead by the extent of acceptable electrical losses as the electrical characteristic of either switch degrades with increased frequency.

$$Figure\ of\ Merit = \frac{1}{2\pi R_{on} C_{off}}$$

**Table 2-1.** Summary of important characteristics for different switch types.

TABLE I

MICROWAVE SWITCH DEVICE PERFORMANCE COMPARISON

| Device Type | $R_{on}$ (ohms) | $C_{off}$ (fF) | FOM-Cutoff Freq. (GHz) |
|---|---|---|---|
| GaAs MESFET | 2.3 | 249 | 280 |
| GaAs pHEMT | 4.7 | 80 | 420 |
| GaAs p-i-n Diode | 5.6 | 420 | 730 |
| Metal Membrane Capacitive | 0.4 | 35 | >9000 |

## 2.3 Reliability

Contact resistance and its stability in ohmic contact switches is one of the least understood characteristics of MEMS devices. This characteristic is also one of the most important and influential in the field. Contact resistance stability and reliability have become almost synonymous as instability is the primary mode of failure for these devices. Another failure mode is the sticking together or adhesion of contacts. The sticking together of the contacts affects both ohmic and capacitive switches, but in different manners. In fact, adhesion in the capacitive switch represents the main mode of failure.

### 2.3.1 Contact Resistance

The issue with contact resistance is maintaining stability over the entire mechanical lifetime of a switch. The problem is that after a number of actuations, the resistance increases without bound, going beyond its design specifications [45]. Lifetime is measured by the amount of time a part can function within a given tolerance, which is set by the dynamics of the circuit and the amplitude of the signal. The threshold is a limit on how much loss the signal can experience before it looses its information. Parts fail when their contact resistance goes beyond the threshold. Figure 2-3 illustrates this

phenomenon. Initially, the switch takes time to settle to a stable value. It remains at this value for the majority of its lifetime. Eventually, the resistance begins to increase exponentially until it exceeds the threshold. At this point, the switch has stripped the information away from the signal and cannot be processed. The need, then, is to extend the lifetime of a switch characterized by the contact resistance as close as possible to the full mechanical lifetime.

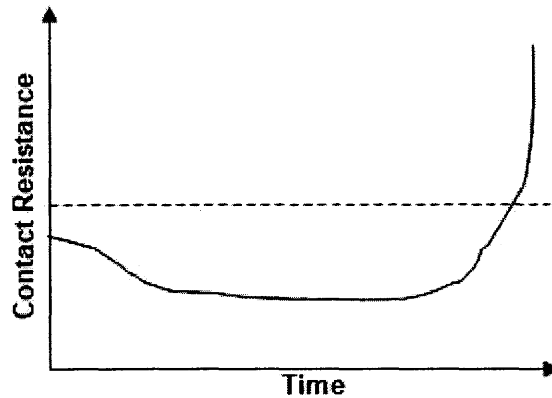


**Figure 2-3.** Contact resistance over time.

Switches designed to handle low power have a longer lifetime than those designed to handle higher power. The single pole single throw (SPST) switch made by Radant MEMS shows that lifetime decreases as input power is increased in both the cold and hot switched case [51]. Lifetime decreases from $10^{11}$ down to $10^{3}$.

### 2.3.2 Stiction

A second common mode of failure for switches involves the sticking together of parts. In this phenomenon called stiction, the contact surfaces remain stuck together. In ohmic switches, the contacts can become welded shut via material deformation caused by high forces or temperatures. Stiction plays a small role compared to contact resistance. In capacitive switches, charges can become trapped in the dielectric material as a result of high electric fields. The effect is the same in an ohmic switch, but is called adhesion instead of stiction. Even when no voltage is applied, the trapped charges are enough to attract the structure and keep it actuated. The onset of stiction is accompanied by increased contact resistance. For RF MEMS to become a viable switching technology, MEMS will need to address this issue. Even if stiction and adhesion cannot be entirely avoided, the number of cycles before this mode of failure occurs should be increased.

## 2.4 Typical Characteristics

MEMS devices boast a number of great characteristics, so do other switch technologies like PIN diodes and optofets. In this work superlatives such as fast, slow or high will be used to describe switches. These words are meaningless, however, unless they are compared to other values. A low loss switch is only low when compared to the loss of another switch. Also, what one person might deem as low another might consider high. For this reason, typical values for characteristics ranging from actuation voltage, to power consumption and RF losses are presented below.

The values in Table 2-2 are compiled from academic literature and data sheets for products currently on the market. Values for RF losses are determined at the limit of the frequency range. For example, the 20dB return loss for MEMS is determined at 10GHz, the upper limit of typical device operation. Values vary across the spectrum. This is important from a design perspective. Depending on the type of characteristics needed for an application, one switch might be better suited than another. In particular, for an application requiring low on state resistance a PIN diode could not be used, but for one needing low actuation voltage it can.

**Table 2-2.** Typical values of characteristics for different switch technologies.

| **Parameter** | **MEMS** | **PIN Diode** | **OptoFET** | **Semiconductor** |
|---|---|---|---|---|
| **Voltage (V)** | 20 - 80 | 0 - 5 | 1.1 – 3.5 | 0.5 – 5 |
| **Current (mA)** | 50 – 250 | 3 - 20 | 1 – 5 | 0.02 – 3 |
| **$R_{on}$ (Ω)** | <1 | 10k | 0.75 – 10.5 | 50 |
| **Power Consumption** | 0 - 20μW | 5 - 100mW | 0.4 - 1 W | 0.05 – 15mW |
| **Power Handling (W)** | | | | |
| **Cold Switching** | 0 – 4 | 0.1 – 1 | 0.15 – 0.9 | 0.25 – 2 |
| **Hot Switching** | 0 – 4 | 0.05 – 0.5 | 4 – 24 | 0.15 -1.3 |
| **Switching Speed (μs)** | 5 – 100 | 1.5 | 100 – 400 | 0.01 - 2 |
| **Freq. Range (GHz)** | DC - 10 | 0.5 - 8 | DC – 100 | DC – 5 |
| **Return Loss (dB)** | 20 | 11 | | 20 |
| **Insertion Loss** | .5 | 3 | | 1.5 |
| **Isolation Loss** | 12 | | None | 40 |

In addition to presenting typical values, Table 2-2 will be used to compare the results for RF losses obtained from the models of equivalent circuits in Chapter 6.

# Chapter 3

# Mechanics

Formal analysis for the operation and characterization of the RF MEMS switch and its limitations begins with modeling the two different switch types, both mechanically and electrically. There are various designs for RF MEMS switches, but all are variants on the beam and cantilever structures. As with any model, the precision is determined by the application that it addresses. However, the goal here is to obtain insight into device behavior. The analysis, therefore, will rely on analytical formulas to characterize as precisely as possible device operation without using computational methods or simulation software.

The dynamics of RF MEMS switches can be analyzed using mechanical models. When applying these models it is important to describe how the structures move and what factors affect movement. Currently the mechanical models aim to account for the non-uniform gap distance that occurs largely in the beam case and less significantly in the cantilever, and a more precise value for the effective spring constant ($K_{eff}$) that depends on mass and dimensions (since this spring constant directly determines displacement).

The investigation of this work is focused not on the mechanics of RF MEMS devices, but rather on understanding how the mechanics affect the electrical characteristics of a device. Formulas for the effective spring constant can be used to calculate the pull in voltage and the capacitances of the on and off states for any material given its properties. In addition, one can calculate the dimensions or properties of a material given a specification of the actuation voltage or capacitances. The formulas used are in standard MKS units unless otherwise specified.

General models for the beam and cantilever switches are illustrated below. These models come from work on obtaining more accurate closed form pull-in voltage expressions [3,8]. Unlike previous work, these models incorporate effects such as axial stress, non-linear stiffening and fringing fields in determining the effective spring constant, which is then used to calculate pull-in voltage. Although Pamidighantam gives models for both structures in [3], Chowdhury's work in [8] is more accurate and is therefore used to describe the fixed-fixed beam.

## 3.1 Fixed-Fixed Structure (Capacitive switch)

Fixed-fixed beams can have net residual stresses as a result of the fabrication process. The presence of this form of stress causes bending of the beam. Axial tensile stress increases the bending stiffness of the beam. Residual stress can lead to a beam bucking upwards or downwards. The stiffness of a fixed-fixed beam under compressive residual stress can be zero if the stress reaches the Euler buckling limit. The entire beam will always buckle in the same direction. For small deflections, it is assumed that axial stress does not change as the beam length changes during loading. When a beam experiences large deflections, however, both axial and transverse displacements must be taken into account. In the large deflection regime, beam bending consists of two components. There is a linear small deflections bending term proportional to the moment of inertia. The other component is a nonlinear stretching term proportional to the product of width and thickness of the beam. Thicker beams are more likely to be dominated by the bending term and thinner beams by the stretching term. The transition from bending to stretching occurs when the deformation of the center of the beam has exceeded the thickness of the beam. Also, if the deflection is large and there is a net residual stress, then an additional source of strain energy results from the residual stress, affecting the linear stiffness term. All of these effects are considered and incorporated into the variational method used by Chowdhury.

Figure 3-1 shows the basic model for the fixed-fixed beam used in Chowdhury's work. When actuated by an electrostatic force, the beam experiences a nonuniform force profile.

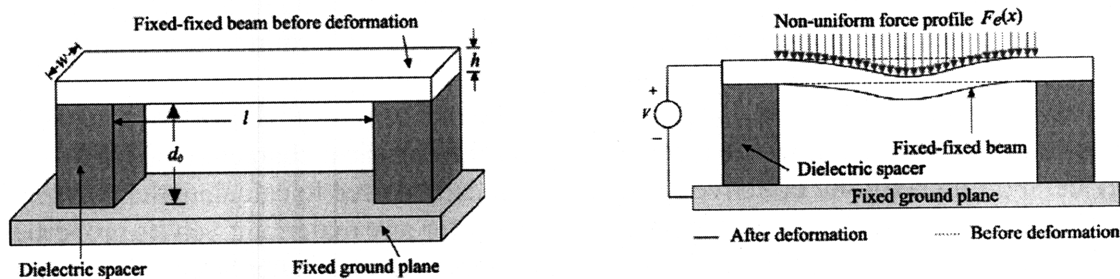


**Figure 3-1**. Structural model of the fixed-fixed beam at rest and when actuated.

To simplify the analysis various assumptions are made. To start, l » w, so that shear stresses near the fixed supports can be neglected which allows the stress in the beam to be approximated as purely uniaxial along the length. It is also assumed that the structure has negligible stress gradient along its length. Third, the structure operates in a vacuum, as to ignore atmospheric loading. Lastly, the width of the supporting dielectric spaces is large enough so that any fringing fields originating at the ends of the supports do not influence the deflection of the suspended length of the beam.

Chowdhury carries out his analysis in the following way. First, he approximates the fixed-fixed beam actuator as a parallel plate capacitor actuator. This allows him to discern an approximation for the capacitance of the structure based on beam deflection. Then he linearizes the electrostatic force about the rest position of the center of the beam.

The manipulation, he states, results in a virtually planar beam that is parallel to the fixed ground plane like the top plate of a parallel actuated actuator. Lastly, Chowdhury compensates for the error in assuming a parallel plate scheme by introducing a compensation factor determined by finite element analysis and a sensitivity analysis of the terms involved. The end result is an expression for the electrostatic pressure:

$$P = \left\{ C_r \left[ \frac{\sigma_0 h}{l^2} \right] + C_b \left[ \frac{E h^3}{l^4} \right] \right\} c + C_s \left[ \frac{E h}{l^4} \right] c^3$$

where P is the applied uniform pressure, $\sigma_o$ is the built in residual stress, E is Young's modulus, and c is the deflection of the center of the beam. The remaining terms are unitless constants derived from finite element analysis: $C_r = 9.35$, $C_b = 32.36$, and $C_s =$ 24.35

As the effective spring constant is the pressure divided by the displacement, it can be found by dividing the expression for P by c.

$$K_{eff} = \frac{P}{c} = \left\{ C_r \left[ \frac{\sigma_0 h}{l^2} \right] + C_b \left[ \frac{E h^3}{l^4} \right] \right\} + C_s \left[ \frac{E h}{l^4} \right] c^2$$

The above expression shows that the effective spring constant consists of two constant terms and one deflection dependent term. For small deflections, the deflection dependent term can be neglected. In the case of large deflection, the last term becomes significant, leading to nonlinear spring hardening.

It is clear from the expression that there are dependencies on the physical dimensions of the device. What is not clearly reflected is that the values for Young's modulus and the residual stress also depend on the dimensions of the device.

A beam is considered wide when w>5h. In this case, the effective Young's modulus becomes the plate modulus expressed as $E = E/(1-v^2)$. The residual stress also changes, to s $\sigma_o = \sigma_o(1-v)$ as given by the Bernoulli Euler limit. A narrow beam is one for which w<5h. Young's modulus remains as E. The fringing fields increase with decreasing width to air gap ratio. For very small ratios fringing fields can actually increase the overall capacitance.

## 3.2 Fixed-Free Structure (Ohmic switch)

The fixed-free model by Pamidighantam is displayed in Figure 3-2. It is similar to the model for the fixed-fixed structure, with two exceptions. First, the load is not symmetric. Second, instead of the largest deflection occurring in the center of the structure, it now occurs at the free end. The values for the model are as follows. Actuation is the result of a distributed transverse load $q_0$. Based on the horizontal position on the cantilever, x, the

beam experiences a certain deflection, y, where the largest displacement experienced by the cantilever is denoted as $y_{max}$. The horizontal distance over which the load acts is $l_c$ and the ratio of $l_c$ as compared to the entire length of the cantilever is $\lambda_r$. The effective stiffness is denoted as $K_{CF\text{-}eff}$ and is composed. The effective stiffness is denoted as $K_{CF\text{-}eff}$. The expression for stiffness of the fixed-free beam is simplified to a large extent by the absence of axial forces (4).

$$K_{CF-eff} = \frac{2}{3}\frac{\hat{E}bh^3}{l^3}\left(\frac{3}{8-6\lambda_r-\lambda_r^3}\right)$$

where Ě is defined as:

$$\hat{E} = \begin{cases} E & b \approx h \\ E/(1-\nu^2) & b > 5h \end{cases}$$

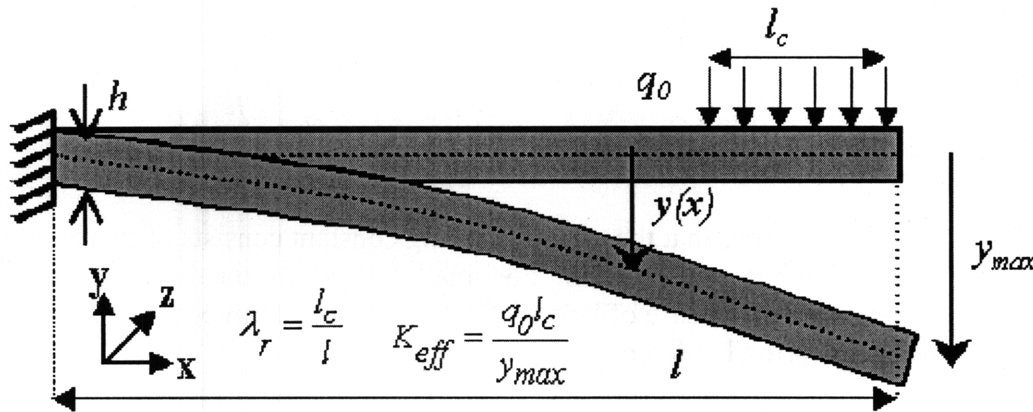


**Figure 3-2**. Fixed-Free beam subject to a partially distributed load $q_0$ ($Nm^{-1}$).

## 3. 3 Switching Speed

Switching speed can be estimated by measuring the time taken by a switch to make the output signal reach a steady state value starting from the point in which the actuation voltage is applied. The time it takes for a switch to actuate (off to on) and release (on to off) is generally different. Due to the hysteretic nature of the switch, release time is less than actuation time. [13] The mechanics of the structures explained above is responsible for determining the dynamics of switching speed.

The importance of switching speed, like other parameters considered in MEMS devices, is that it determines the types of applications in which it could be used. Capacitive switches, which suffer currently from microsecond switching, cannot be used in high-speed applications like transmit/receive switching [5, 22]. As a result, capacitive switches are used only statically.

There has been progress in terms of increasing the mechanical switching times for capacitive switches. Fast capacitive switches, however, are nothing new. In 1999, Yao in his work of low loss micromachined switches, showed actuation times of 6μs and release time of 4μs. This good switching speed was offset by the high actuation voltage of 50V needed to produce these fast times.

The figure of merit has been to improve switching time while also improving other parameters, to the end goal of a creating a better switch. In 2005, Park obtained switching times of 5us using a multiple contact MEMS switch whose insertion and isolation losses were only slightly less than those reported by Yao but whose pull-in voltage was 35V [23].

# Chapter 4

# Electrical Modeling

## 4.1 Capacitive Switch

Recall that the capacitive switch functions by providing low loss between input to output when in the on state and shunting a signal to ground in the off state. The structure of the switch is a beam bridge across a CPW transmission line. The nature of switch in the on state where one metallic structure is separated from another by a fixed distance is described by a capacitor. The contact area is defined as the overlapping area of the beam and the transmission line illustrated in Figure 4-1a. The down state (off) can also be modeled by a capacitor, with the distance between contacts being that of the dielectric thickness. Figure 4-1b shows the down state. In this state the signal is being shunted to ground.

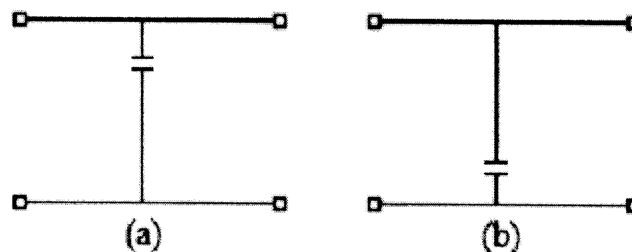


**Figure 4-1**. Conventional (a) on state and (b) off state impedance model of the capacitive shunt MEMS switch.

## 4.2 Ohmic Switch

The basis of the ohmic switch is a cantilever which separates input from output. In the off state there is no electrical connection. The contact area of the cantilever is isolated from the contact area of the wire by air. Separation of these two contacts effectively forms a capacitor with a distance equal to the gap spacing. In the on state, the cantilever contacts the wire forming a resistive path between input and output. The resistivity of the path is related to the length of the wire trace and the material from which it is made. The on and off states are shown in the figure below, Figures 4-2a and 4-2b.

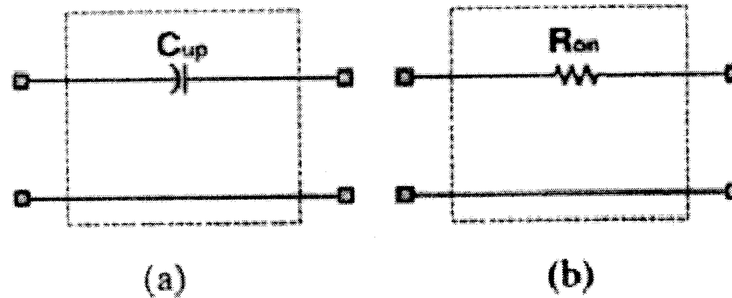


**Figure 4-2**. Conventional (a) off state and (b) on state series impedance model of the ohmic contact MEMS series switches.

## 4.3 Parasitics

In order to create a better RF model for both switch types we consider what parasitics might exist in the models that have not yet been included.

### 4.3.1 Capacitive Switch

As the signal becomes shunted to ground, it experiences some resistive and inductive losses. The resistive loss arises from the signal dissipating energy through the ground line and the substrate. A small parasitic inductance is also present from the loop the circuit forms. The value of inductance will be somewhere between the case of a single loop solenoid or a single turn of wire.

In total then, more than just having a capacitor we also have a resistor and inductor in series. Figure 4-3 is taken from the work by Kobayashi [14] on a high fidelity RF MEMS capacitive switch. Most of the device behavior is determined by the down state capacitance. For extremely high frequency characterization, these parasitics should be included, but they will be omitted in this work.

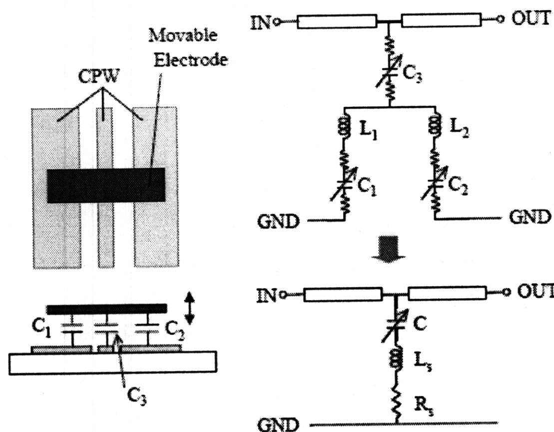


**Figure 4-3.** Basic layout of the capacitive MEMS shunt switch. The right side shows the equivalent circuit and the simplified model.

### 4.3.2 Ohmic Switch

Two parasitics for the ohmic switch are fringe capacitances, which appear in both the on and off states, and an inductance that occurs when the switch is in the on state.

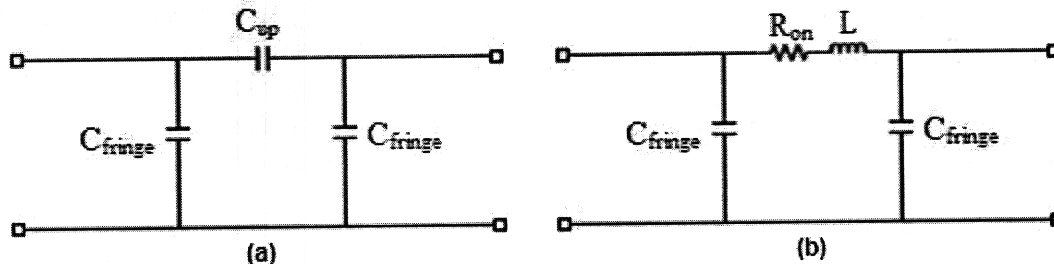


**Figure 4-4.** Parasitics for the (a) up and (b) down state of the ohmic switch.

The parasitic capacitances are the result of fringing fields the transmission line (explained in section 4.4). As the same lines are used in both states, the fringing capacitances appear in each.

Jaewoo was able to discern the presence and value of these parasitic elements using the parameter extraction technique based on the dimensions of the switch structure and line geometries [55]. He found the fringing capacitances have a value of 22fF and the inductance a value of 65pH. For purposes of simulations and exploring the behavior of any ohmic switch, these parasitics should be included. Knowing that they must be included is not enough, the values also need to be known. One method that could be used to approximate these values is by scaling. To first order, the capacitance should directly scale with Jaewoo's area and inversely with his reported distance. The inductance could be approximated by the formula of a one turn loop. The value would scale directly in relation to the length and height of Jaewoo's cantilever and inversely with the width of his line.

Using an area of 5μm x 50μm, $\varepsilon_r = 10.9$ for GaAs, and substrate thickness of 625μm leads to an approximation for fringing field capacitance of 3.5fF. Although compared to the reported value of 22fF, the approximation is off by a factor of 6, it is still very close to what was reported. As Jaewoo's results were corroborated, scaling could be used to obtain reasonable estimates.

With a loop area of 0.5μm x 90μm and line width of 50μm, the inductance is calculated to be 2.03pH. Compared to the value reported, this estimate is off by a factor of 30, an error five times greater than that for the estimate for capacitance. The estimate for the inductance is not great. Instead of relying on an estimate from this first order model to determine values from any geometry, the 65pH reported in Jaewoo should be taken to be a baseline from which inductances for other switch geometries can be scaled.

## 4.4 Transmission lines

The switch is not a standalone device. We need some way to interface the device inside a package to the outside circuitry or electronics that might use it. That is, we need some way to send to the switch an input signal and pass an output signal from the switch back to the larger circuit. Thus far, the models presented for the on and off state of the ohmic and capacitive switch have assumed no electrical connections were needed to connect the switch to the circuit. Transmission lines, which form the basis of the electrical connections in the MEMS regime, help us perform this task.

In the macroscale, wires and electrical connections are assumed to have essentially no impact on the circuit itself. Although these do have some resistance, it is more or less negligible when compared to components that comprise the rest of the circuit. In transitioning to the microscale, effects that we ignore in the macroscale actually become quite important. For some applications, the milliohms worth of resistance of a connection might represent a large fraction of the resistance of other devices. Impedance matching is a critical design issue. Input and output impedances must be matched to efficiently deliver power to the circuit. Long wires can add unwanted parasitic inductance to a circuit, thus affecting high frequency response. As attenuations change based on frequency, wires should remain stable across the operational bandwidth.
In short, transmission lines must serve the dual role of providing electrical connection while minimally affecting the circuit.

Transmission lines are implemented as flat conducting surfaces over the substrate of the wafer. The two main types are microstrip and coplanar wave guides. Equations have been developed by Hilbert [15], Wheeler [16], Schneider [17], Hammerstand [18] and others for coplanar waveguides and microstrip structures. These allow one to calculate the dimensions needed for a particular line impedance or to alternatively calculate the line impedance that results from a set of given dimensions.

Over the years, the models presented have evolved into CAD software which use numerical methods to handle more of the complexity that arises from geometries and

solve Poisson's equations much more exactly. While software has enabled designers to understand their design, software has also assisted in modifying the same closed form expressions that have served as the foundation for these. Curve fitting and parameter extraction have led to very simple yet accurate closed form expressions. Modifications also refine the effects of frequency on dispersion, attenuation, and its effects on the characteristic impedance and effective dielectric constant. Closed form expressions, however, should not just be used by themselves since they only provide results to assist in the design that can later be studied more in depth with the use of software. To the extent of this work, these closed forms will provide extremely useful results.

### 4.4.1 Extent of effects

One might ask how much of an extent these structures depend on frequency and if it is significant enough to merit the consideration. If the results including frequency compared to the quasistatic case show little variation then why bother with including it. The short answer is yes.

In studying the propagation of picosecond pulses, Frankel noted just how severe these effects can be. Figure 4-5 shows the results of Frankel's work. As a signal travels down a line, it can experience frequency spread, amplitude attenuation and suffer from distortions. The original signal, a sharp impulse at the start, turns into an ill defined impulse taking the shape of a sine wave.

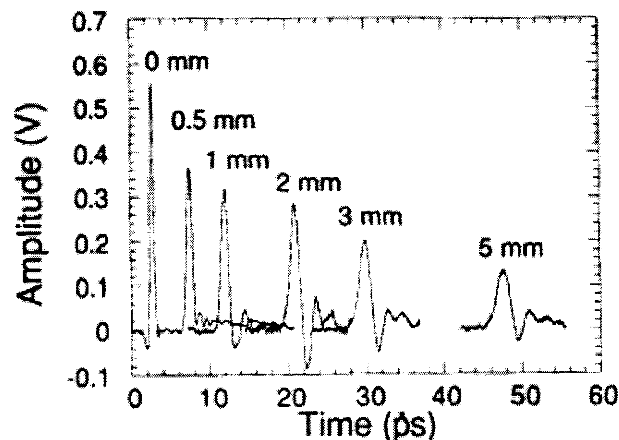


**Figure 4-5**. Typical time domain picosecond pulse propagation.

Frankel also compared his models to actual experimental data for effective permittivity and attenuation, which are displayed in Figure 4-6. In doing so he managed to highlight two points. First, that there are indeed frequency effects which must be considered. In the plots both the permittivity and attenuation increase with frequency. The second is that the models he presents model the observed data very well. This can be seen in the small variation exhibited between the calculated and measured data.

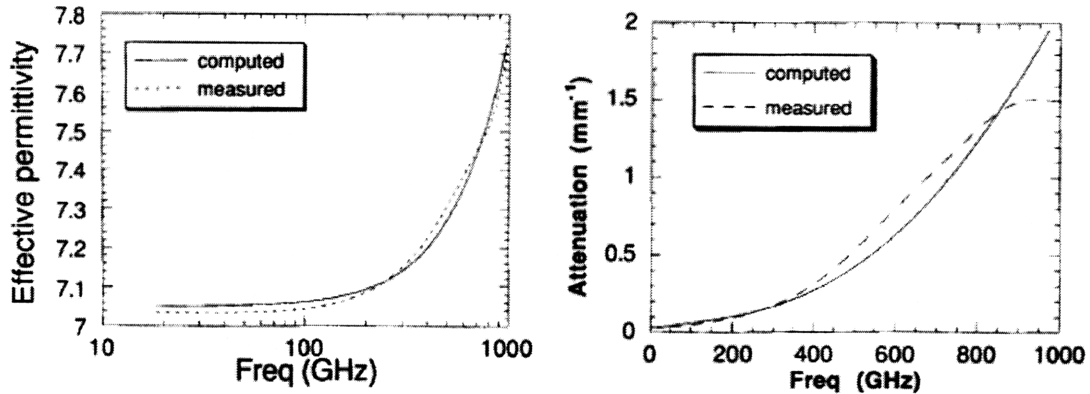


**Figure 4-6**. Effective permittivity and attenuation for a CPW line on GaAs substrate with $a = 1840$ and $f_{te} = 43\text{GHz}$.

Geometry of the transmission lines also plays a role. There is a great deal of variation as illustrated below. The effective dielectric constant is displayed as is varies across various width to height ratios and across different frequencies. On the whole, for a particular design, the w/h ratio of the wire, as well as the signal frequency, significantly impact the behavior of the wire.

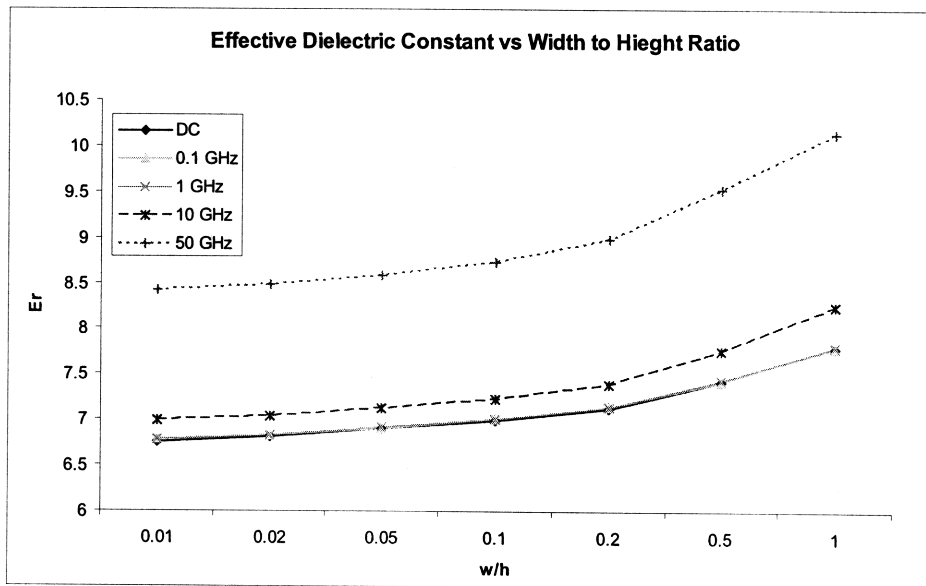


**Figure 4-7**. Effective dielectric constant versus width to height ratios with operation from DC to 50GHz.

Figure 4-7 illustrates several key points:

- There is little variation on the $\varepsilon_{eff}$ from DC to 1GHz, regardless of the w/h ratio
- Including the w/h ratio for this range, the variation across 2 orders of magnitude for w/h is only 15%. At 10GHz, the variation across all w/h ratios is 19%; at 50GHz it is 20%.
- As the frequency increases, the effective dielectric constant approaches the dielectric constant of the substrate, in other words, $\varepsilon_{eff} \rightarrow \varepsilon_{eff}$. This is attributed to the increased concentration of the field within the dielectric at higher frequencies.
- Widths and heights cannot be made to be any arbitrary ratio. Synthesis equations, present later in this work, govern which width to height ratios are needed for to obtain a particular characteristic impedance.

The limitations on device operation not only include the switch and its associated parameters but also the behavior of the electrical connections from device to package. What is desired of a switch is just to prevent or allow a signal to show pass from input to output, not completely distort it. For this reason, excluding the dependence would lead to inaccurate and perhaps misleading results and insight when characterizing the RF performance of the MEMS switch in the following section.

### 4.4.2 Microstrip Transmission Line

A microstrip transmission line is the simplest structure for creating electrical connections on a wafer. One can consider the connection itself a flat wire as it is merely a conductive metal layer deposited on top of a substrate. This flat wire structure is represented in Figure 4-8 below.

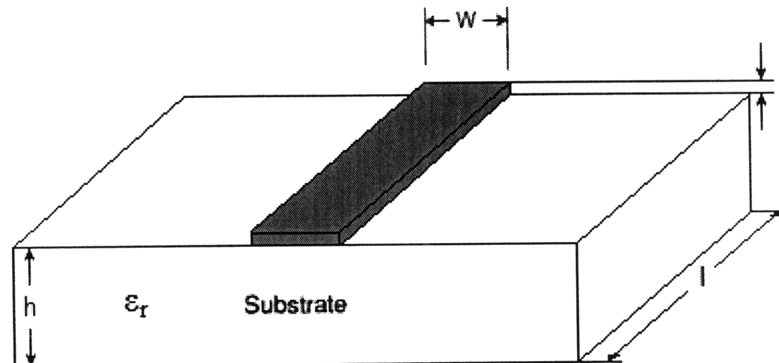


**Figure 4-8**. Microstrip configuration.

Our goal here is to understand how the addition of these wires to the circuit will affect the model. For purposes of analysis, we will denote the width of the signal line as (w), the length of the wire (l) the thickness of the layer (t), the depth of the substrate (h) and the dielectric constant of the substrate ($\varepsilon_r$). Using these parameters we can define the effective dielectric constant ($\varepsilon_{eff}$) and characteristic impedance of the line ($Z_o$). The effective dielectric constant describes the interaction between the permittivities of the

wire and the substrate. Since the wire and substrate will be different materials, the interactions of the two permittivities must be accounted for. Ultimately, the effect of the wire is described by the characteristic impedance. Due to the dependence of the dielectric constant on the calculation of the characteristic impedance, this value can then be found.

The expressions that have been developed to account for frequency use conformal mapping. A derivative of Maxwell's laws is that electric fields must be perpendicular to any metal surface. In transmission lines, the fields that occur from the side walls of the structure, i.e. the fringing fields, curve from the surface as they traverse from air to the substrate dielectric. Wheeler and others were able to capture the dynamics of fringing electric fields by using conformal mapping to treat these curve paths linearly.

The derivations contain elliptic integrals with solutions called elliptic functions. K(k) and K'(k) used in the equations represents a complete elliptic function of the first kind and its complementary function, respectively. These functions can be evaluated in Matlab, or as presented in equation 1.45 in Russer and Biebl, approximated to within 10 parts per million by:

$$\frac{K(k)}{K'(k)} = \begin{cases} \left[\frac{1}{\pi}\ln\left(2\frac{1+\sqrt{k'}}{1-\sqrt{k'}}\right)\right]^{-1} & \text{for } 0 \le k \le \frac{1}{\sqrt{2}} \\ \frac{1}{\pi}\ln\left(2\frac{1+\sqrt{k'}}{1-\sqrt{k'}}\right) & \text{for } \frac{1}{\sqrt{2}} \le k \le 1 \end{cases}$$

$$K'(k) = K(k') \text{ and } k' = \sqrt{1-k^2}$$

The elliptical functions almost always appear as a ratio. Where equations include products in place of ratios, the Matlab command K = ellipke (M) can be used. Note, the convention within matlab is to use M as the moduli of the complete elliptic integral instead of k; to find M, simply square that value of k.

The following equations can be found in Russer and Biebl as with the equation above. They are included for reference. To find the dispersive behavior of the microstrip line, the quasi-static values must be found first.

The characteristic impedance of a microstrip line is represented as:

$$Z_{o,eff} = \frac{Z_o(\varepsilon_r = 1)}{\sqrt{\varepsilon_{r,eff}}}$$

where the effective dielectric constant $\varepsilon_{r,eff}$ takes into account the ratio of the field in the air to the field in the substrate. It is valid over the range $0.01 \le w/h \le 100$. For $\varepsilon_r = 1$ the characteristic impedance is:

$$Z_o(\varepsilon_r = 1) = 60\ln\left[F\frac{h}{w} + \sqrt{1 + \left(\frac{2h}{w}\right)^2}\right]$$

and

$$F = 6 + (2\pi - 6)\exp\left[-\left(30.666\frac{h}{w}\right)^{0.7528}\right]$$

where F represents a term found by functional approximation to the exact values found by conformal mapping.

Within the range $1 \leq \varepsilon_r \leq 128$, the effective dielectric constant can be found using:

$$\varepsilon_{r,eff} = \frac{\varepsilon_r + 1}{2} + \frac{\varepsilon_r - 1}{2}\left(1 + \frac{10}{w/h}\right)^{-ab}$$

with a and b defined as:

$$a = 1 + \frac{1}{49}\ln\left[\frac{\left(w/h\right)^4 + \left(\frac{w/h}{52}\right)^2}{\left(w/h\right)^4 + .432}\right] + \frac{1}{18.7}\ln\left[1 + \left(\frac{w/h}{18.1}\right)^3\right]$$

$$b = 0.564\left(\frac{\varepsilon_r - .9}{\varepsilon_r + 3}\right)^{0.053}$$

These equations, provided that both w/h and $\varepsilon_r$ are within the specified ranges, are accurate to within 0.2% of the exact result using computation methods.

Using the values obtained from the above expressions, the frequency dependence can be found. Over the range $2 \leq \varepsilon_r \leq 16$, $0.06 \leq w/h \leq 16$ and $0.003 \leq h/\lambda \leq 0.3$, the equations have an error of less than 3%.

The effective dielectric constant as it varies with frequency

$$\varepsilon_{r,eff}(f) = \left(\frac{\sqrt{\varepsilon_r} - \sqrt{\varepsilon_{r,eff}}}{1 + 4F^{-1.5}} + \sqrt{\varepsilon_{r,eff}}\right)^2$$

where:

$$F = \frac{4h}{\lambda}\left(0.5 + \left[1 + 2\log\left(1 + \frac{w}{h}\right)\right]^2\right)\sqrt{\varepsilon_r - 1}$$

$$\lambda = \frac{c}{f}$$

The frequency dependence of the characteristic impedance is given by:

$$Z_o(f) = Z_o\frac{\varepsilon_{r,eff}(f) - 1}{\varepsilon_{r,eff} - 1}\sqrt{\frac{\varepsilon_{r,eff}}{\varepsilon_{r,eff}(f)}}$$

where $Z_o$ represents the quasistatic value of the characteristic impedance.

### 4.4.3 Coplanar Wave Guides

Coplanar wave guides (CPW) are an extension of the microstrip design. In place of one metal strip, a CPW transmission line is composed of three metal layers on the same plane. In this configuration, illustrated in Figure 4-9, the line that carries the electrical signal is in between two ground planes on either side. The width of the signal line is denoted as (w), the length of the wire (l), the thickness of the layer (t), the spacing between the ground plane and signal line (s), the depth of the substrate (h), and the dielectric constant of the substrate ($\varepsilon_r$). The important part about this configuration is not so much the width of the ground planes, but rather the separation between these and the signal line. Of note, as the ground planes are closer to the signal line, CPW have improved isolation over the microstrip design.

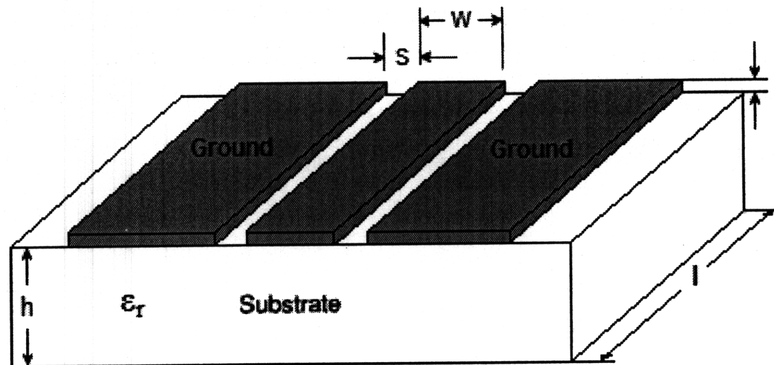


**Figure 4-9**. CPW configuration.

The analysis for the CPW of transmission line is carried out the same as before. We first need to obtain the effective dielectric constant in order to calculate the characteristic impedance. Since the structure of the conducting surface is different, the formulas are different as well.

Excellent work on characterizing the frequency dependence on characteristic impedance and effective dielectric constant was performed by Frankel in his study of terahertz attenuation and dispersion of picosecond pulses on coplanar transmission lines made of Ti/Au on a GaAs substrate [19]. His work presents models in agreement with experimental data up to 0.9THz. Again, while the formulas can be found in his work, they are presented below for reference.

First, find the frequency dependence on the effective characteristic impedance.

$$Z_{cpw} = \frac{120\pi}{\sqrt{\varepsilon_{\mathrm{eff}}(f)}} \frac{K'(k)}{4K(k)}$$

where k is the ratio of line width to overall distance between ground planes, expressed as:

$$k = \frac{w}{w + 2s}$$

The effective dielectric constant is given by:

$$\sqrt{\varepsilon_{\text{eff}}(f)} = \sqrt{\varepsilon_q} + \frac{(\sqrt{\varepsilon_r} - \sqrt{\varepsilon_q})}{\left(1 + a(\frac{f}{f_{te}})^{-b}\right)}$$

where b ≈ 1.8 and $\varepsilon_q$ , *a* and $f_{te}$ are calculated as:

$$\varepsilon_q = \frac{\varepsilon_r + 1}{2}$$

$$\log(a) \sim u\log\left(\frac{w}{s}\right) + v$$

$$u \sim 0.54 - 0.64q + 0.015q^2$$

$$v \sim 0.43 - 0.86q + 0.54q^2$$

$$q = \log\left(\frac{w}{h}\right)$$

$$f_{te} = \frac{c}{4h\sqrt{\varepsilon_r - 1}}$$

By itself, $f_{te}$ represents the cutoff frequency of the lowest order TE mode that exists on the line. After this point, other modes bring to propagate on the line. In the equation, it serves to normalize the frequency.

In addition to providing formulas for $Z_o$ and $\varepsilon_{eff}$, Frankel studies attenuation and dispersion, which ultimately lead to modifications of older work on this topic. Attenuation and dispersion the signal experiences in traveling down the line can be found using the following:

$$\alpha_{cpw}(f) = \left(\frac{\pi}{2}\right)^5 2\left(\frac{\left(1 - \frac{\varepsilon_{\text{eff}}(f)}{\varepsilon_r}\right)^2}{\sqrt{\frac{\varepsilon_{\text{eff}}(f)}{\varepsilon_r}}}\right)\frac{(w + 2s)^2\varepsilon_r^{3/2}}{c^3K'(k)K(k)}f^3$$

$$\beta(f) = 2\pi\frac{f}{c}\sqrt{\varepsilon_{\text{eff}}(f)}$$

### 4.4.4 Synthesis

With the proper width, slot and height ratio, a CPW transmission line can be made to have any characteristic impedance. For RF applications, typical characteristic impedances are 50Ω or 75Ω.

There are well known closed form equations that can be used to obtain the ratio needed for a 50Ω line. The synthesis equations in Deng [20] yield very accurate estimates within 1% for widths and heights in place of using a full-wave computer simulation for a structure. Dimensions for transmission lines in the RF performance section will be selected to yield 75Ω for the microstrip structure and 50Ω for the CPW. The difference arises from the large dimensions required to create a 50Ω line in the microstrip case so much so that the structure really ceases to be a MEMS device in the strict treatment of dimensions being tens of microns or smaller. With a substrate thickness of 525um, a microstrip would need to be roughly 140um wide to achieve a characteristic impedance of 75Ω. Alternatively, to obtain a 50Ω line, we would need to increase the width to 425um, or three times the size.

## 4.5 Actuation Voltage

Aside from simply determining the actuation voltage needed to turn the switch on, the importance of pull in voltage lies in the deeper ties it has in the operation of the switch, ranging from lifetime, contact resistance stability, stiction, and power handling capabilities. The pull in voltage is not just important from an electrical point of view. Pull in voltage also determines the dynamic response of the switch. For these reasons, pull in voltage is extremely important.

### 4.5.1 Conventional first order model

To begin, let us start with a model of the switch, deriving an expression for the pull in voltage. Armed with this equation, we can draw insight between the relationship of pull in voltage and device operation.

To first order, both a cantilever and beam switch is modeled as a pair of parallel conducting plates that form a capacitor, with a free end and a fixed end. Although the membrane in a beam switch exhibits non uniform displacements (the center moves than the edges) meaning the mechanics are somewhat different than a cantilever, the same relation holds for either switch, namely the balance between a mechanical restoring force and an electrostatic force. This is displayed in **Figure 7**. The plates have an effective overlap of $A_{eff}$ separated by a distance d. The top plate is suspended by a spring with a stiffness of $k_{eff}$ meant to model the mechanical restoring force of the beam $F_m$. When a DC voltage is applied between the two plates, an electrostatic force $F_e$ is created. The electrostatic force causes the gap distance to decrease. The two plates will remain an electrical open circuit while the electrostatic force balances the restoring force of the beam. As soon as the electrostatic force exceeds the restoring force, the plates come together and the switch closes.

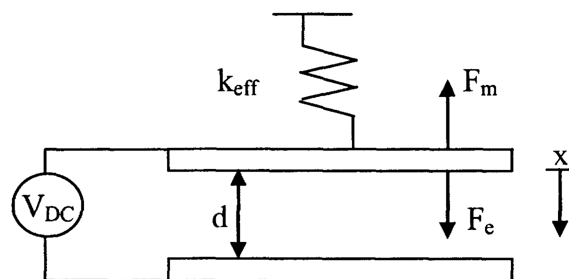


**Figure 4-10.** Parallel plate capacitor model of an RF MEMS switch.

For large width to length ratios, the mechanical restoring force exerted by the free electrode in this first order model can be represented as the force of a spring with spring constant $k_{eff}$:

$$F_m = -k_{eff}\, x$$

The electrostatic force of the movable plate can be found by taking the derivative of the stored electrical energy in the capacitor with respect to the displacement of the plate.

$$U = \frac{1}{2} C V^2$$

$$F_e = -\frac{d}{dx} U = -\frac{d}{dx}\left(\frac{1}{2} C V^2\right) = \varepsilon_0 A_{eff} \frac{V^2}{2(d-x)^2}$$

It is interesting to observe that while the mechanical restoring force varies with linearly with x, the electrostatic force varies as the inverse square of x. These two forces $F_m$ and $F_e$ will exactly balance, either when a constant DC voltage is applied or when the signal varies slowly in time. Thus, the force balance equation is:

$$-k_{eff}\, x = \varepsilon_0 A_{eff} \frac{V^2}{2(d-x)^2}$$

To find the pull in voltage, we simply rearrange the above equation. Simple manipulations yield:

$$V = \sqrt{\frac{2k_{eff}}{\varepsilon_0 A_{eff}} x(d-x)^2}$$

At some point, the mechanical restoring force can no longer balance the electrostatic force. When this occurs, the gap distance immediately goes to zero and the free electrode collapses on top to the fixed electrode, thereby closing the switch. The phenomenon is called snap through. The deflection after which snap through occurs can be found by taking the derivative of the pull in voltage with respect to x and finding when it is zero.

As reported in the literature, this deflection that leads to snap through is exactly d/3 or 1/3 of the original gap spacing. The pull in voltage that leads to this deflection is solved for by substituting d/3 into our equation for V:

$$V_{pull-in} = \sqrt{\frac{2k_{eff}}{\varepsilon_0 A_{eff}} \frac{d}{3}\left(d-\frac{d}{3}\right)^2} = \sqrt{\frac{2k_{eff}}{\varepsilon_0 A_{eff}} \left(\frac{d}{3}\right) d^2 \left(1-\frac{1}{3}\right)^2} = \sqrt{\frac{2k_{eff}}{\varepsilon_0 A_{eff}} \left(\frac{1}{3}\right) d^3 \left(\frac{4}{9}\right)}$$

$$= \sqrt{\frac{d^3 k_{eff}}{\varepsilon_0 A_{eff}} \left(\frac{8}{27}\right)}$$

From the above equation, we can immediately see what parameters affect the pull-in voltage. There is a linear dependence on the spring constant $k_{eff}$, a cubic relation on gap distance and an inverse relationship with the overlap area of the electrodes $A_{eff}$. At first pass, to have a switch with low $V_{pull-in}$, we want a material with a small spring constant, low gap spacing and high overlap area.

### 4.5.2 Refined Model

If the beam and cantilever structures strictly behaved as parallel plate capacitor, then the first order model would suffice to predict pull in voltage. The reality is that device operation is much more complicated that the typical model used. Nonlinear stiffening, charge redistribution and fringing fields mar the simplicity of just parallel plate actuation.

The highlights of the previous section on mechanics were equations for accurate calculation of the effective spring constant of a fixed-fixed beam and fixed-free beam. These can be used to derive a refined expression for the pull in voltage.

For the fixed-free beam, Pamidighantam's equation for effective spring constant can be plugged directly into the first order equation for pull in voltage.

Almost the same manipulation can be done for the fixed-fixed beam. It turns out that there is a subtle nuance for the critical deflection of the center for pull in for the fixed-fixed beam structure is 4/10 of the initial gap rather than the 1/3 ratio of the fixed-free beam. However, the 1/3 deflection of the original gap distance can still be used even though the actual deflection of the center is a little bit more than this. Chowdury equates the electrostatic pressure to the elastic pressure and solves directly for the pull in voltage. The result:

$$V_{PI} = \sqrt{\frac{\left\{C_r\left[\frac{\sigma_0 h}{l^2}\right] + C_b\left[\frac{Eh^3}{l^4}\right]\right\} \cdot \frac{d_0}{3} + C_s\left[\frac{Eh}{l^4}\right] \cdot \left(\frac{d_0}{3}\right)^3}{\varepsilon_0\left(\frac{5}{6d_0^2} + \frac{0.19}{d_0^{1.25}w^{0.75}} + \frac{0.4h^{0.5}}{d_0^{1.5}w}\right)}}$$

From Chowdhury's equation the effects of all device parameters can be seen. As expected, the results show the dependence on the material properties. More importantly, the relation incorporates the physical dimensions of the device. Length, width, and height are accounted for unlike the first order model which has excluded these.

These modifications included, just how good are the models? The fixed-free case has much more variation from software simulation than does the fixed-fixed case. Pamidighatam reported variation from CoventorWare ranging from 3.4-11.1% The extent of the error is deceiving; the actuation voltages calculated were all less than 4V as shown in Table 4-1.

**Table 4-1.** Extent of errors in [3].

| | | | | | |
|---|---|---|---|---|---|
| Pamidighatam | 2.33 | 0.84 | 1.33 | 2.07 | 3.83 |
| CoventorWare | 2.25 | 0.75 | 1.2 | 2.3 | 4 |
| **% Error** | **3.43** | **10.71** | **9.77** | **11.11** | **4.44** |

Chowdhury's relations exhibit less fluctuation. For the small deflection regime there is a maximum deviation of 1.27% between his results and those obtained from FEA. Maximum deviation for large deflection is just 2%. Lastly, for the case of extreme fringing fields, the results differ by just 0.5%. In his work Chowdhury notes that percent error also differs between different FEA software.

### 4.5.3 Other considerations

A corrugated bridge has much lower residual stress over a flat bridge, as shown by Song in making his corrugated bridge capacitive switch. Also, thinner bridge thickness yields lower values. Halving the thickness from 1um to 0.5um lowers the residual stress to a third of the initial value. The analysis considers these results to lower the actuation voltage [11].

There is a strong temperature dependence on the actuation voltage of a switch. Noel et al discovered that as the ambient temperature was decreased to absolute zero the actuation voltage increased. This is due to the strain and stress of the material that serves as the beam and the difference in the coefficients of thermal expansion between the beam and the substrate [10].

## 4.6 S-parameters

The essence of the switch model is to determine return loss, insertion loss and isolation loss, the three important electrical characteristics that govern the RF performance of the switch. These values stem directly from the behavior of signals as waves and can be quantified by S parameters.

The S parameter representation can be used to characterize any RF network with any number of ports. Typically, RF and microwave networks consist of a cascade of two or more two-port networks. In this case, it is convenient to define a 2 by 2 transmission, of ABCD matrix, for each two-port network [21]. Any two-port network can be characterized by multiplying together the ABCD matrices of the smaller two-port networks of which it consists. With the ABCD matrix of the overall two-port network, the S parameters can be calculated by using the equations as found in table 4.2 on page 211 of [21] and turn into a decibel loss by multiplying by 20 the log base 10 of the magnitude of S.

The S parameter representation of the return loss is $S_{11}$. Return loss is a measure of how much of the incident from the source is reflected back to the source. The extent of the reflected wave is due to mismatches in impedance between what the incident wave sees

at the input boundary of the circuit. Due to the frequency dependence of circuit components, the resistance seen, and thus the return loss, also depends on frequency. It is expressed in decibels (dB). This value should be as small (as negative on a dB scale) as possible.

Insertion loss, expressed as $S_{21}$, represents the attenuation a signal experiences as it travels through the circuit from input to output. From a power standpoint, insertion loss describes how much of the transmitted power is seen at the load. Ideally, while one would like to see all of the transmitted power at the load, a fraction is lost. Expressed as a ratio, insertion loss is always less than 1 (negative in dB). For good characteristics, insertion loss should be kept close to 1 (0 in dB).

Isolation loss can be thought of as the converse of insertion loss. Instead of looking at how much of the input signal is seen at the output, isolation loss describes how much of the signal at the output is seen at the input. We find isolation loss as the transfer function from output to input. Isolation loss describes the extent that a switch behaves as a switch in the off state. The isolation is measured by $S_{21}$ along the signal line with no applied voltage bias.

## 4.7 Complete Device Model

Having discussed the general behavior of the ohmic and capacitive switch, the parasitics that appear for each model, and the need to include transmission lines to describe the electrical connections into and out of the device, the complete models are now presented.

### 4.7.1 Ohmic Switch

For the off state of the ohmic switch, we have the same capacitive network that included the capacitor from input to output and capacitors to capture the effects of fringing fields. Additionally, we have a transmission line that attaches to the input side of the switch and another which attaches on the output side. The complete model is shown in Figure 4-11.

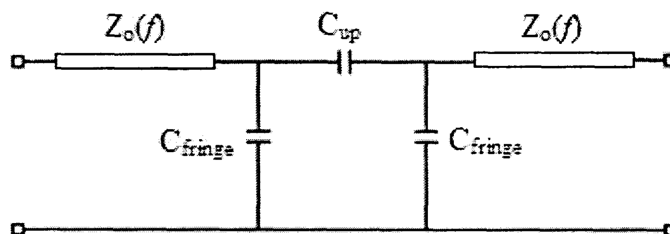


**Figure 4-11**. Complete off state model of the ohmic switch.

The on state of the ohmic switch looks the same as before, with the only change being that there is now a transmission line on the input and output side. Figure 4-12 displays this modification.

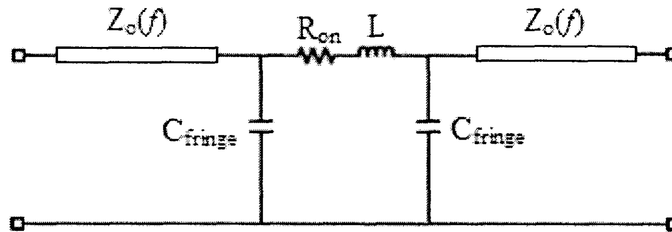


**Figure 4-12**. Complete on state model of the ohmic switch.

### 4.7.2 Capacitive Switch

Most of the device behavior is determined by the up or down state capacitance. For extremely high frequency characterization, the parasitic resistor and inductor shown in [14] should be included, but they will be omitted in this work. The models, then, look almost like the simple first order models initially presented. The up state of the device, or rather on state, is described by a shunt capacitor flanked by a transmission side on either side as in Figure 4-13. The off state, shown in Figure 4-14, has the same configuration, where the up capacitance is replaced by the down capacitance.

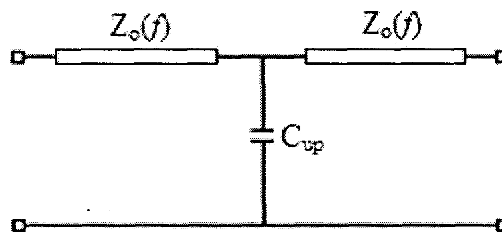


**Figure 4-13**. Complete up state model of the capacitive switch.

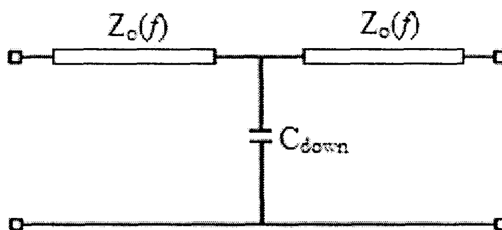


**Figure 4-14**. Complete down state model of the capacitive switch.

### 4.7.3 ABCD Matrix and Losses

To analyze the switch, the ABCD matrix for the network must be found. The T network in either state is a combination of three parts: the transmission line, a shunt capacitor and another transmission line. Each has a simply ABCD matrix representation. Multiplying the three together, the overall ABCD matrix is found to be:

$$ABCD_{up} = \begin{bmatrix} \cos(\beta l) & jZ_o(f)\sin(\beta l) \\ jY_o(f)\sin(\beta l) & \cos(\beta l) \end{bmatrix} \begin{bmatrix} 1 & 0 \\ j\omega C_{up} & 1 \end{bmatrix} \begin{bmatrix} \cos(\beta l) & jZ_o(f)\sin(\beta l) \\ jY_o(f)\sin(\beta l) & \cos(\beta l) \end{bmatrix}$$

$Z_o$ and $\beta$, the characteristic impedance and electrical length, respectively, appear in the calculation and reflect the frequency dependence of the device.

Losses in the up state include return ($S_{11}$) and insertion loss ($S_{21}$). They relate to the ABCD matrix in the following manner:

$$S_{11} = \frac{A + B/Z_0(f) - CZ_0(f) - D}{A + B/Z_0(f) + CZ_0(f) + D}$$

$$S_{21} = \frac{2}{A + B/Z_0(f) + CZ_0(f) + D}$$

where A is the upper left (1,1) entry in the $ABCD_{up}$ matrix, B is the upper right (1,2) entry, C is the lower left (2,1) entry and D is the lower right (2,2) entry.

Isolation loss ($S_{12}$) is found from the ABCD matrix in the down state. This matrix is identical to the up state matrix with $C_{up}$ replaced with $C_{down}$:

$$ABCD_{down} = \begin{bmatrix} \cos(\beta l) & jZ_o(f)\sin(\beta l) \\ jY_o(f)\sin(\beta l) & \cos(\beta l) \end{bmatrix} \begin{bmatrix} 1 & 0 \\ j\omega C_{down} & 1 \end{bmatrix} \begin{bmatrix} \cos(\beta l) & jZ_o(f)\sin(\beta l) \\ jY_o(f)\sin(\beta l) & \cos(\beta l) \end{bmatrix}$$

Then, $S_{21}$ is calculated from this matrix as:

$$S_{12} = \frac{2(AD - BC)}{A + B/Z_0(f) + CZ_0(f) + D}$$

with A, B, C and D defined as before.

As it stands, all of the losses are complex numbers with real and imaginary parts. To convert this into a loss, expressed in decibels, we take the magnitude of the S parameter. Then the log base ten of the magnitude is multiplied by 20.

# Chapter 5

# Current Work

RF MEMS switch work has taken many different routes aside from the creation of a single good switch. On the fore front of current work is reliability, with investigations tackling the issues of contact resistance, stiction and dielectric breakdown. System integration, new materials, and fabrication techniques are other areas where considerable advancements have been made.

Given the work that has resulted from the introduction of the first RF MEMS switch in 1991 [1], what is the current state of the art? Fifteen plus years of academic and industry investigations has led to deep understanding about certain aspects of MEMS devices and hardly any understanding about others.

Significant strides have been in the area of material research, for example. For MEMS devices, the need to understand residual stress in materials due to fabrication processing has led to new measuring techniques. Baek et al developed a technique that uses the resonance method to measure the natural frequency of a fixed-fixed beam from which residual stress can be extracted using Rayleigh's energy method. To ameliorate fabrication stress gradients, Sedky et al, present a pulsed laser annealing approach. Reliable and accurate material characterization like Poisson's ration can be carried out by a double membrane bulge test. What is more, new materials have been developed and studied to obtain higher mechanical performance based on material characterization techniques like these. Silicon nitride ($SiN_xH_y$), polysilicon germanium (SiGe) or silicon carbide (SiC) are all examples.

However, there still remain areas for which investigations have not been able to uncover much, if any, significant insight. This is the case for contact resistance for which the mechanisms that cause the eventual increase explained before still remain foreign. The causes of adhesion are only slightly better understood.

## 5.1 Contact Resistance

Investigations into this issue have studied the problem by looking at the effects of different contact materials, the impact on the contacting surfaces of localized intense electric fields, the dynamics of thin insulating films that can build up, or the role of contact force in determining contact resistance. One does not need to be well versed with

these issues to guess the results of such studies: materials with lower resistivity (like metals) have lower contact resistance; intense electric fields can lead to sparks that can char the surface; any debris on the surface or films that insulate it, will serve as a barrier to flow causing an increase in resistance; more area will come into contact as the surfaces are slammed harder into each other, leading to a decrease in resistance.

Common sense often plays a large role in providing insight. But as mentioned, the mechanisms which increase contact resistance still remain cryptic. While the use of gold contacts lowers the initial value of the contact resistance, gold contacts still suffer from an eventual exponential increase in resistance. Even when intense electric fields are lowered, by way of a stepped actuation voltage like in Figure 5-1, the resistance increases [45]. Insulating films can still occur in devices packaged in a hermetic environment (free space filled with an inert gas) by way of outgassing of impurities from the package seal or the eventual diffusion of impurities from the bulk of the contact up to its surface. Lowering the contact force, despite the effect of increasing the actuation voltage and value of the contact resistance, only delays the eventual increase of resistance.

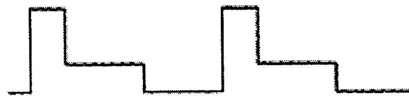

**Figure 5-1**. Dual pulsed actuation waveform. The initial large pulse serves to provide the actuation voltage needed to move the structure. Once in motion, the voltage is lowered to mitigate otherwise large intense electric fields.

Rather than provide concrete answers, literature on the work for contact resistance proposes methods to ameliorate the effects. In this way, the problem of the stability of contact resistance can be worked around, but not resolved. Although these methods do not serve to contribute much to the field of theory on the workings of contact resistance, they do contribute insight to the design of switches. A design engineer can assuage the problems of resistance by implementing redundancy into the design of the switch. Instead of creating one great switch with a long lifetime via long contact resistance stability, an engineer can create a series of independently good switches, using results from literature such as low contact force, hermetic sealing, and low resistivity metals, and cascade them together. Along with some detection circuitry, then an overall switch failure would result when all of the cascaded switches fail.

Despite the lack of concrete answers, there is still extremely interesting work in the field which might help pinpoint more precisely what is going on. Two pieces of work that stand out are the heating of contacts and the modeling of contact geometry.

Self heating of contacts can occur when a high enough electric field is established across the small separation distance of the contacts, or from the friction that results when the contacts are slammed together during actuation. In any case, self heating is important as it affects the resistance of the contacts. Aside from self heating, the contacts can experience heating effects from the substrate.

Jensen et. al looked at the effects of substrate heating on contact resistance. To observe the effects, Jensen used a thermal stage to slowly heat the substrate of a switch from room temperature to 90°C at a rate of 6°C per minute, recording the resistance during heating. What he found was that the contact resistance decreased with increased chip temperature, depicted in Figure 5-2. From the figure, it is clear that as the substrate is heated, the contact resistance drops from a maximum of 70Ω down to 3Ω. Most of the drop in resistance occurred from 60-70°C with very little reduction after 70°C. This threshold seems to indicate there is an optimal point, or temperature, after which there are diminishing marginal returns. Jensen explains this reduction in resistance is caused by contact heating called contact softening, with true contact softening occurring in the surfaces heated sufficiently to cause annealing of dislocations in the contact.

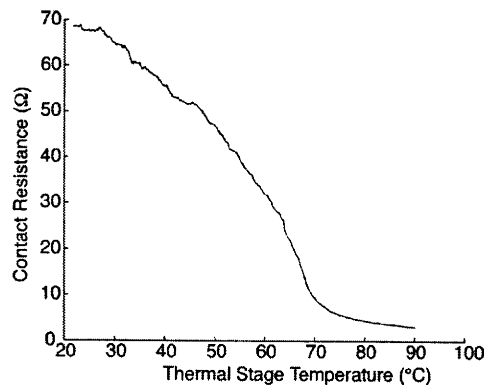


**Figure 5-2**. Decrease in contact resistance with temperature increase in chip substrate.

As it applies to switch design, Jensen's work is important in two ways. First, similar drops might occur for nominal resistances of 1ohm. Jensen's work did not study switches with such low contact resistance but future work might reveal a similar behavior. If so, then switches can be made to have less fluctuation in their resistance, hopefully contributing to increase reliability. The second important point is that substrate heating could be incorporated into a design for extremely low contact resistance.

Also investigated was the time dependence on contact resistance. Jensen performed an experiment in which he waited several days between subsequent actuations of the switch. When not under test, the switches were stored in a vacuum. He found that even with only a few actuations on the days the switches were actuated (the switches were actuated 5 times) there was an increase in contact resistance. While Jensen speculates that the cause for the increase is the gradual build-up or repair of an insulating film, only the presence of impurities is likely to cause the large change in contact resistance, seen in his work. Previous work indicated that sputtered gold films most likely retain a thin insulating layer, probably composed of hydrocarbons absorbed onto the surface. This idea is supported by the high contact resistance of switches prior to a burn in cycle. Sufficient voltage placed across the contact can break down this insulating layer and both lower and stabilize the contact resistance.

Modeling contact surface is another facet of contact resistance investigations. So much of contact resistance has to do with the roughness of the surface that it is important to

detail work in this area. When two contacting surfaces come together, the electrical connection between them is formed by the high points on each surface, producing a real contact area a finite number of spots called asperities. Jensen shows a simple illustration of how the contact forms a connection. For reference it is displayed in Figure 5-3.

In his work, heating causes the contact asperities to grow after a connection has been made. Growth of the contact spot leads to a larger contact area and lower resistance. Certainly this is another reason why contact resistance decreases after a burn in cycle. However, actuation once this connection has been made can lead to an increase in contact resistance rather than just a low stable resistance. Insulating thin films still play a role in contact resistance. Even after an insulating film has been removed by a high enough voltage, which creates a conducting contact spot, contact resistance can increase. Randomness in the closing process of the switch can cause the film-free contact spots to be misaligned on the first actuation after the spot had been established. This action, in turn, can press film onto the edges of film free areas, promoting the regrowth of film, thus increasing the contact resistance. This behavior, Jensen hypothesizes, seems to explain why there appears to be just one real contact spot. With so much area that can contact when a switch closes, having one real contact spot seems very unlikely.

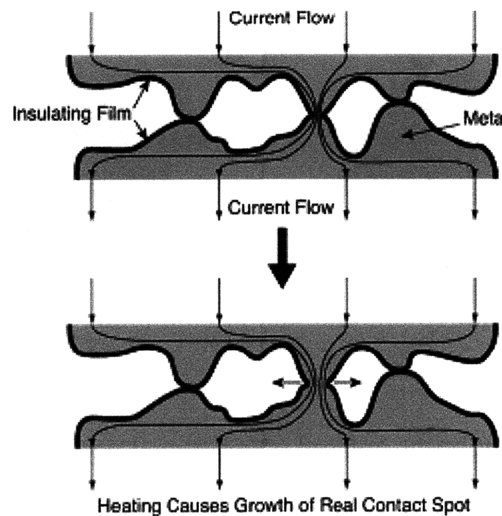


**Figure 5-3**. Contact asperities in contact surfaces.

The surfaces of the contacts in MEMS switches, or any other material for that matter, are not smooth in an absolute sense. Surfaces are rough, have spikes and edges, a direct result of the fabrication process of materials. Instead, surfaces should be envisioned as sandpaper. There is coarse sandpaper and fine sandpaper. While one is smoother than the other, both are abrasive, and thus rough.

Ideally smooth surfaces have been researched to propose numerical models and analytical methods to describe the contact mechanics. Some probabilistic models that have been proposed account for asperity height variations [54]. However, studies such as these do not account for the actual surface topographies related to the roughness of the contacting surfaces; Jensen's work touches on it only slightly. Since current flow is limited to these

regions where contacts touch, it is important to have an accurate representation of the contact area for predictions on contact resistance.

The random nature of surface roughness can be better modeled using fractal geometry. The real area of contact, contact pressure and resistance has been related to surface roughness as a result of this approach. Work conducted by Rezvanian gives better perspective as to what actually occurs.

Rezvanian recognized that contact resistance depends on the area of the contacting spots, stipulating the need to have an accurate model for the area very important for characterization. Fractal geometries can be used to generate the random topographies common to a wide range of MEMS devices. Figure 5-4 shows the 3D fractal representation of the surface roughness of a contact produced by Rezvanian using a Weierstrass-Mandelbrot function. The second contact is assumed to be perfectly smooth, with all the variation existing in the generated model. This representation is then used to predict the thermo-mechanical asperity deformations of contacting surfaces over time, where contact resistance is assumed to vary by softening effects due to localized heating and strain hardening.

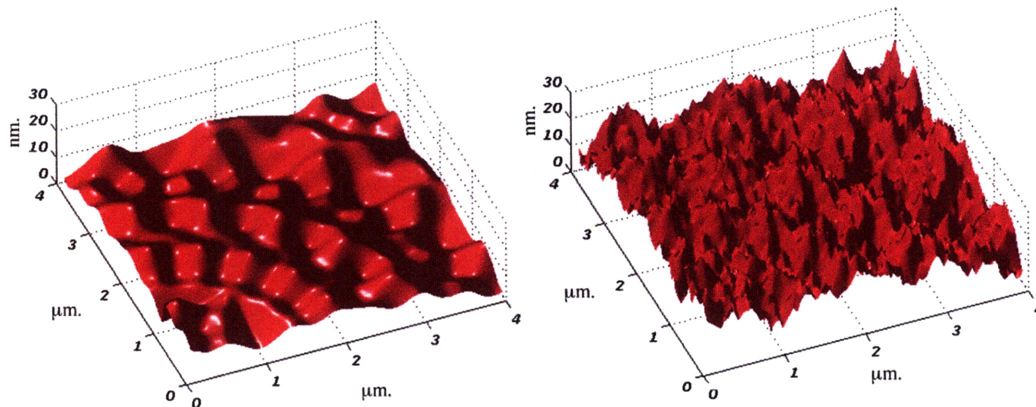


**Figure 5-4**. 3D surface roughness created using fractal geometry. The model on the left has a peak to valley height of 12nm (rms of 7.2nm) while the model on the right has a peak to valley of 27.1 (rms of 14.9).

Using this generated model, Rezvanian obtained rather significant results. First, high initial pressure of the switch leads to a steep increase in contact area for the first couple of actuations of a device. These high pressures lead to large deformations in the contact asperities, which in turn lower the applied pressure. The deformation of asperities results in more asperities coming into contact with each other. As a consequence, the real surface area of the contacts increases. Strain hardening and the decrease of applied pressure reduced the rate of increase of contact area.

The second finding is perhaps the most significant. In studying the number of contact spots over the first 48 hours of switch actuation, the real contact area is roughly only 7% of the apparent area as shown in Figure 5-5. Out of the entire 4µm x 4µm contact, there were roughly 40 contact spots. The resistance of the contact is then only actually

determined by a small fraction of the total area involved. This result suggests that there is really only a pseudo dependence of contact resistance on area. A larger contact area might only have a marginal number more of contact spots than a smaller area, meaning that the contact resistance between them might be similar instead of very different. But the number of contact spots also depends on the roughness of the surface, not just on the size of the contact area. In the figure of number of contact spots, we see that the first model with lower peak to valley distance has a lowers number of spots, 7, for the same area as the model with a peak to valley distance of 27.1 that has 40 spots.

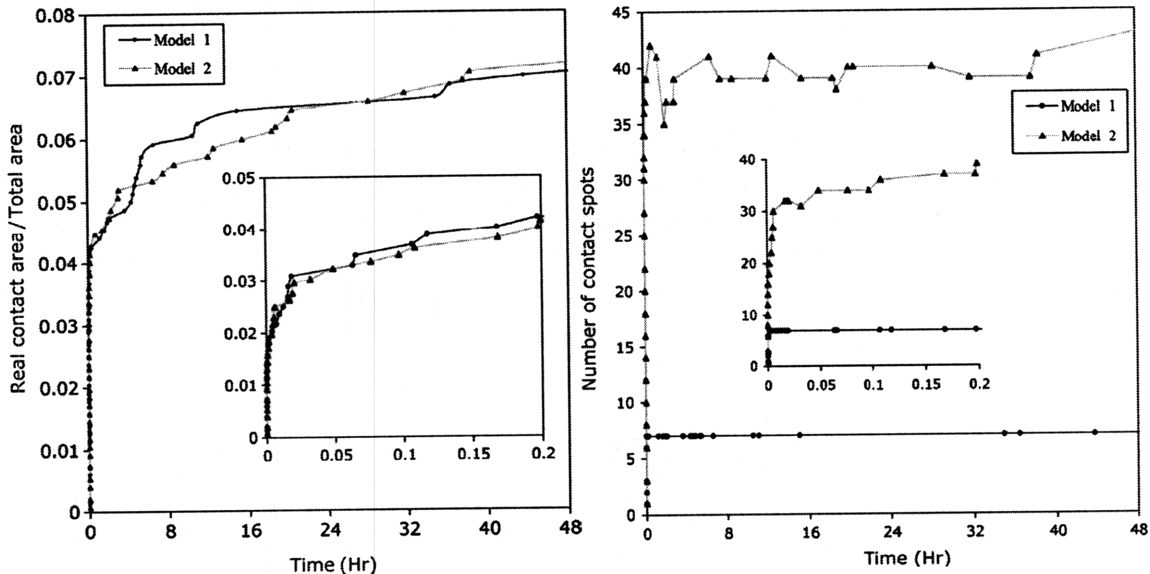


**Figure 5-5.** Real contact area and number of contact spots as a function of time of device operation.

The researchers, as with this author, are careful to point out the shortcomings of the investigations. Jensen notes that while his low cycle experiments cannot prove that the lifetime of a MEMS switch can be extended, the results show that contact heating may be used to avoid the important failure mechanism of increased contact resistance.

In looking closer at the data above, the results seem to increase slightly towards the end of the time period under consideration. The real contact area experiences continued increase, never settling on a steady-state value after initial increase within the first couple of actuations. Although the number of contact spots for the simpler geometry remains constant, the number of spots for the more complex structure increases. It could be that there time period is not long enough to show a steady-state, and that there are effects which a longer period would show. From the standpoint of insight and extrapolation, a 48 hour trial seems long enough to illustrate a bulk of the effects. Alternatively, regardless of the increase at the end of both plots, the real contact area is less than 10% of the total area, and the number of spots for the complex geometry is small.

Other things to keep in mind is that homogeneity of material reduces variation of contact resistance between subsequent cycles, contact resistance depends on the kinds of particles forming at the contact constriction at any given moment

As strange as it may be, contact resistance actually as dependence on the closure rate of the contacts. In a study of silicon oil contamination on gold contacts by Dickrell the closure rates of the contacts were varied from 40nm/s to 400nm/s. In measuring the resistance of the gold contacts, Dickrell discovered that the slower the contacts come together the more rapidly the contact resistance increases. This behavior is illustrated in Figure 5-6. The increase in contact resistance across all closure rates occurs in steps. This is most easily seen in the 400nm/s case where the contact resistance through the first 60 cycles increases slightly, at which point steps to a new stable value, jumping again just before reaching 150 actuations.

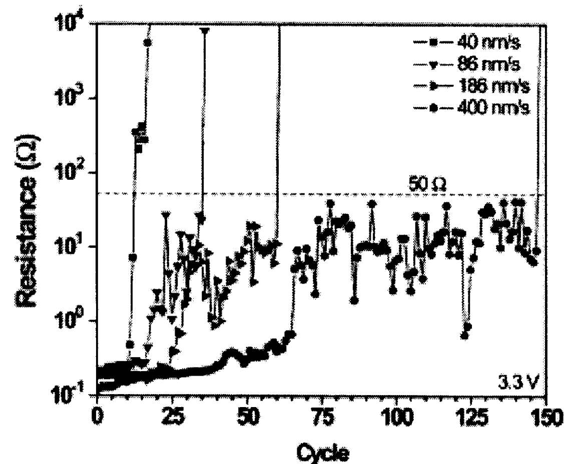


**Figure 5-6**. Dependence of resistance degradation on gap closure rate for an applied voltage of 3.3V.

## 5.2 Stiction

As it stands, there is no real solution to the problems of sticion and adhesion. Work in the area of stiction has led to insight into how to ameliorate the problem. The mechanisms that cause adhesion are better understood through work on thin films.

Monolayer coatings have a positive effect on reducing the wear of surfaces [42]. This work shows that self assembled monolayer coatings have the double effect of reducing stiction and reducing wear. While this is promising indeed, work using silicones as a coating indicate that there might not be a free lunch [43]. In fact, there might be a tradeoff between friction and contact resistance. Silicones have many beneficial properties when applied to surfaces: they promote chemical stability and friction reduction between sliding contacts similar to SAM coatings. However, as noted by Dickrell, silicone oil impairs the performance of electrical contacts through insulating surface film formation and accumulation. Thus, while coatings can be used, its effects on contact resistance should be considered.

Great work on adhesion came from Sune's investigation on thin film $SiO_2$ dielectrics [44]. The work which relates more to dielectric breakdown than on trapped charges. Sune subjected various thin film $SiO_2$ networks to either dynamic of static electrical stress, noticing that the network progressively degrades until a threshold degradation is reached and a new conduction mechanism produces the final effective dielectric breakdown. The degradation is based on the length of time that the oxide layer is stressed. The generation of neutral trapping sites that become partially occupied by electrons is believed to cause the degradation of the thin film. When a certain critical density of defects is locally reached, the breakdown mechanism is triggered at which point destructive thermal effects take over, opening a low-resistance ohmic path between the electrodes. The degradation itself is produced somehow at random over the area of the structure and depends on oxide quality.

The final breakdown spot area is very small, smaller than $10^{-4}$ of the total contact area. The area of the degraded spots that trigger the final run-away breakdown mechanism is found to be on the order of $10^{-13}$ $cm^2$ or $10^{-5}$ $\mu m^2$. This is important for two reasons; the first, is that only a small area needs to be degraded to serve as a conduction path; the second is that the small contact area is in line with the work done on contact spots, illustrating once again how much of the device behavior is determined by small areas. Breakdown, then, seems to be a process with a weakest-link character. So long as one link in the entire chain is broken the device fails. Sune notes

In thin films, two different types of breakdown have been observed. Low field defect-related breakdown describes the short-time period breakdown and high field intrinsic breakdown describes long-time breakdown. There is evidence that breakdown mechanism is always the same independent of the type of stress. Lastly, the experimental distributions for the breakdown mechanisms are found to depend on electrode area giving rise to the notion that the geometry of the layer is an important as the properties of the layer itself.

Dielectric breakdown of insulating films is important, and in the end related in some way to a random mechanism [44]. The comprehension of the breakdown statistics, as noted by Sune, may help better understand the physics of the mechanism of dielectric breakdown which is still unclear.

## 5.3 Switch Designs

A number of different designs have been implemented to obtain good characteristics, whether it be lower insertion loss, lower switching time, lower voltage, etc.

A novel warped-beam capacitive MEMS switch reported from the University of Waterloo shows that by creating a switch with curved electrodes (similar to applying wings off of the center switching structure) down capacitance is doubled and up capacitance is halved. The beams are made from Au-Cr. These wings curve upwards because of residual tensile stress. This curved nature means that the effective overlap

looks less in the up state. In the down state, the curved parts of the beam come into contact with the electrode, effectively creating more area. The benefit is that the improvements in capacitance come without the need to use a thinner dielectric or a material without a higher dielectric constant [34].

Yet another type of RF MEMS switch is created using liquid metal as the contact material. Rather than having gold metal to metal contacts as in a conventional ohmic switch, this switch has liquid to liquid contacts and operates by moving mercury to create an electrical connection. The switch design pales in comparison to other switches having a switching time of 1ms, 1dB insertion loss and better than 20 dB isolation loss at 18GHz. Despite these poor values, the switch has a contact resistance of 70mΩ over 100 million cycles. [35]

As noted already in [36], resonant mode RF switches are being investigated and fabricated in the academic setting. The applications to the field of ATE are not apparent at this time, but for new applications this switching mode could be worthwhile.

Switches with large deflections are reported in [37]. Multiple contact switches, as described in [23] have accomplished lowering insertion losses. Redundancy has also been used to improve reliability [37].

## 5.4 System Integration

Hybrid CMOS- MEMS Integration is one such area of system integration. Combining RF switch and accompanying electronics into one package will save space, drive down costs, and improve RF characteristics.

Integration of MEMS device with the integrated circuit becomes increasingly important for creating high performance compact designs. Current work has been in hybrid CMOS-MEMS design. Advantages with this hybrid approach are shorter development times and independent optimization. This approach, however, suffers from higher packaging costs, foot print area is large, and parasitics due to long interconnects and the size of bond pads, fundamentally affecting RF performance [39]. The true benefit of this technique is monolithic integration.

Monolithic integration of CMOS and MEMS has a number of benefits. The idea is to have MEMS devices rest on top of CMOS. In this way, interconnections are made much shorter and the device much smaller. The CMOS would be processed first and the microsystem last. In order for this scheme to work, processing and fabrication technologies for CMOS and MEMS must be compatible. At present, MEMS are made at much higher temperatures that CMOS are fabricated or can withstand.

## 5.5 New Materials

The foresight of needing new materials that can be processed at lower temperature has paved the way for the design of new materials. More than just lower temperature processing, these materials must have at least similar, if not better, mechanical and electrical characteristics than poly Silicon.

Poly-SiGe is one such material that provides the necessary mechanical properties and reliability required for MEMS applications at a significantly lower temperature compared to conventional poly-Si. The deposition temperatures for poly-SiGe are $<450^{\circ}C$ which contrasts the $>850^{\circ}C$ needed for poly-Si [39]. The concentration of silicon to germanium was known to be to resistive for MEMS applications [40]. Newer findings have shown that poly-SiGe can be deposited at temperatures as low as $210^{\circ}C$ and have resistivities of 80 mΩ per cm [41].

## 5.6 Fabrication Techniques

New fabrication techniques have also been employed. Yoon et al. has fabricated complex 3D MEMS structures using a multidimensional UV exposure scheme. Rather than just exposing SU-8 photoresist to light from one angle, as has been the convention, they have shined UV light at varying angles to create structures that neither bulk nor surface micromachining has realized. The technique has created structures as complex as those seen below in Figure 5-7 and Figure 5-8, a filter and inverted cones.

Up to now only, cantilever and beam switches have been considered. With fabrication techniques such as this, more complicated structures can be created, still based on the same two underlying designs. The potential benefit is that other mechanical properties, like stiffness, might be optimized by way of more complicated designs. It is not necessarily the case complex designs will ultimately lead to a better switch, but having such fabrications scheme might give rise to insights that will.

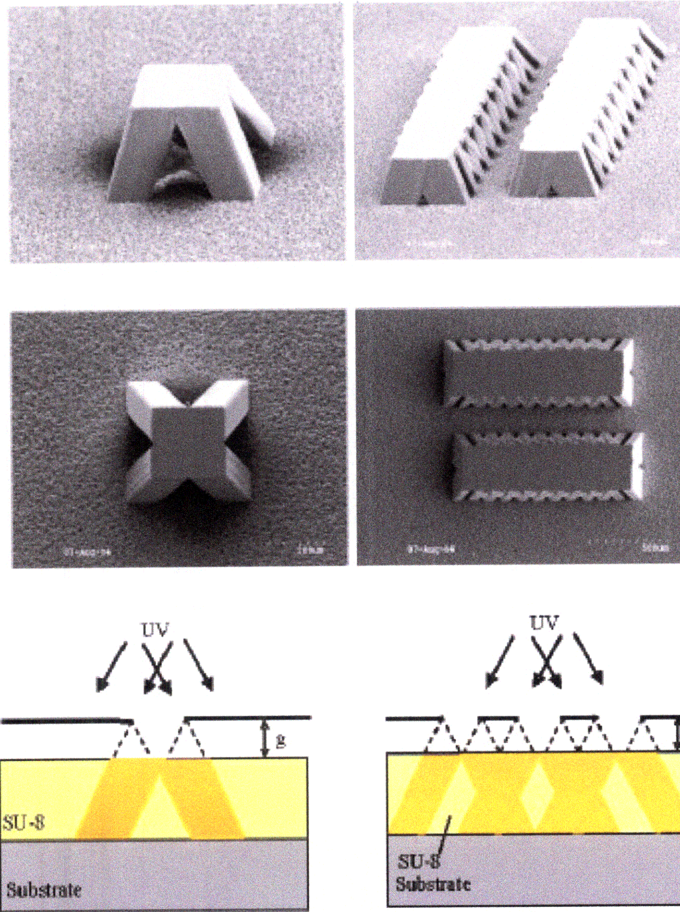


**Figure 5-7.** Complex structures created using multidimensional UV exposure scheme.

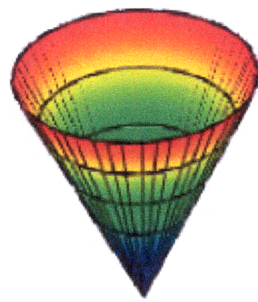

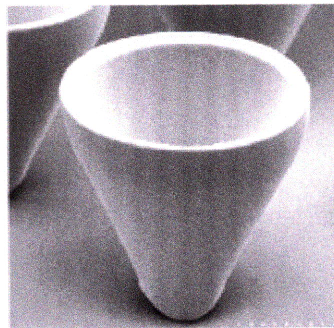

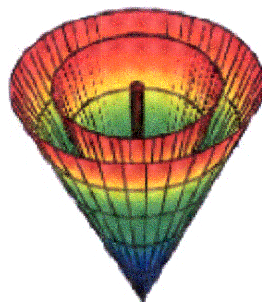

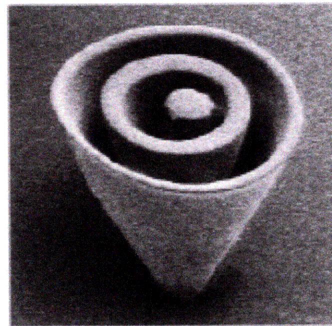

**Figure 5-8.** Concentric cones created using multidimensional UV exposure scheme.

## 5.7 Reliability

The military has been conducting their own reliability tests, and have since 2004, been working on defining standards that can be applied to all the MEMS devices they test and will eventually use [29]. Some of these military standards have been adopted by the MEMS field. MIL-STD-883 has been used by many MEMS studies conducted previously. It is currently used for quality assurance specifications by companies that devices for high volume applications, like Analog Device. MIL-STD-810 defines the testing of the effects of operating, transportation and storage environments.

It is certainly true that the reliability requirements for military application are much more stringent than that of the consumer MEMS field. However, the fact that the military is still working on establishing their own standards, and that some of these have become adopted by the consumer MEMS field illustrates two important points. The first is that the issue of reliability has yet to be pinned down for MEMS as it has been for the IC field from which the latter emerged. The second, until standards are established, now moving away from requirements more so into fabrication and production, not much is going to come of the MEMS field aside from more designs and different structures. The proprietary nature of many MEMS manufacturing and packaging processes, as well as the general immaturity of the industry impedes the development of these needed standards.

High humidity and high shock environments are two operations of high concern in military applications. MEMS also need to stand up to long term storage, where hermeticity must be preserved.

With the numerous different types of MEMS devices, one governing standard might not be possible, but rather various standards, since each class might be characterized by a common failure mechanism or reliability issue, and thus should be addressed accordingly.

# Chapter 6

# RF Performance

The aim of this section is to observe the frequency characteristic of the capacitive switch. On state and off state capacitances of the device determine the frequency behavior and these depend on the insulating material and thickness of the layer, as well as the physical dimensions of the beam structure as determined by actuation voltage. Upon discussing the choices available for these factors, plots for the device obtained by using Matlab are shown.

## 6.1 Down state Capacitance

In the down state, the capacitance of the capacitive switch is determined by the thickness of the insulating layer, the dielectric constant of the layer, and the area of overlap between the beam and the substrate.

For the insulating layer, $SiO_2$ can be used, and in fact deposited as thin as 1.4nm [6]. Thin layers of this sort are typical for creating the gates in FET devices. In the case of $SiO_2$, however, the layer can only be so thin. Below 2nm, electrons can leak through layer, causing leakage currents that rob power away from the device, thus, adversely impacting device operation. The need to lower leakage currents while maintaining high capacitance had pushed the development of high dielectric (high-k) materials. For the same thickness of $SiO_2$, high-k materials yield larger capacitance, precisely what is needed for the down capacitance in a capacitive switch. Despite the limitations in FET devices, $SiO_2$ could be used in creating the thin insulating layer needed for DC isolation in a capacitive switch.

One high-k material that has received a lot of attention has been hafnium oxide. It has a dielectric constant of 30, 8 times greater than $SiO_2$. The drawbacks to the use of hafnium oxide are that it is not straightforward to create and complicated to deposit. Whereas Si02 can be formed by oxidizing the wafer, simple exposure to oxygen, hafnium oxide requires volatile precursors and sophisticated techniques like chemical vapor deposition (CVD) or atomic layer deposition (ALD) to create an insulating layer. Robertson also noted that hafnium oxide has inferior properties compared with $SiO_2$, such as a tendency to crystallize and a high density of electronic defects [6]. These characteristics notwithstanding, hafnium oxide is poised to be the high-k material the industry will adopt [7]. As a result, we will consider it in calculating a down state capacitance.

Another high-k material is lead zirconate titanate (PZT), which compared to $SiO_2$ has a dielectric constant of about 200, making it roughly 50 times greater. This material has been used in conjunction with hafnium oxide to create multilayered dielectrics that have produced high isolation switches [9]. It is worth mentioning this material to note that there are others that could be used to achieve even better results than those presented using hafnium oxide as a baseline.

### 6.1.1 Thickness of Insulating Layer

Previously mentioned was that $SiO_2$ layer can be formed to be less than 2nm thick. This presented problems for the FET case. For MEMS we care about shunting a signal to ground, where leakage currents are less of a concern. Assuming that the DC bias signal does not short to ground with a thickness of 2nm, the analysis will be performed for a hafnium oxide of this thickness.

The down state capacitance is easily found by the capacitance formula $\varepsilon_r\varepsilon_o A/d$. With a d =2nm, A = $(100\text{nm})^2$, $\varepsilon_r = 30$, and $\varepsilon_o = 8.85419*10^{-12}$ F/m, hafnium oxide gives a down capacitance of 1.33nF where a $SiO_2$ layer of the same thickness is 8 times less, or 173pF.

## 6.2 Up State Capacitance

To first order, $C_{up}$ can be calculated in the same way as $C_{down}$. This capacitor has the beam as the top plate and the top portion of the insulating layer as its bottom plate. The separation of the plates is the total gap minus the thickness of the insulating layer. With no medium in between the plates, just free space itself, this capacitor has the free space permittivity of $\varepsilon_o = 8.85419*10^{-12}$ F/m.

Including the effects of $C_{down}$ in the calculation, $C_{up}$ is 44.314fF. The ratio of on to off state capacitance is just under 30,000. In comparison, just using Si02 as the insulating layer, the up state capacitance is 44.31fF giving an on to off state ratio of 3,900. Though this ratio might seem high, it is in line with results presented in literature. Off capacitance is usually on the order of tens of femptofarads and on capacitance in the order of picofarads [13].

There is a subtle difference between the calculation of the up state and down state capacitance. A careful eye might notice that due to the spacing in the down state, fringing fields could be assumed negligible. In fact, it is the same assumption made in electrostatics for finding the capacitance between two plates. The finite thickness of the beam will contribute fringing fields. Thus, while the fringing fields could be ignored in the down state, they cannot in the up state.

Up state capacitance is actually the sum of three capacitances: the parallel plate capacitance, the fringing field capacitance due to the beam width, and the fringing field

capacitance due to the thickness of the beam. For high values of width to dielectric thickness, the fringing fields have a small impact on the total capacitance, meaning they can be neglected. For width to dielectric thickness smaller than 1.5, the fringing fields become more significant, leading to an overall increase in capacitance by a factor of 1.5 to 3 [8].

Precise characterization of the up state capacitance can be performed using parameter-extraction methods that which would include the use of a network analyzer. The value using this method would account for all of the dimensional properties of the beam. In [8] Chowdhury presents a formula to calculate $C_{up}$ including the effects of fringing fields that were included in the pull in voltage thereby saving the trouble of using a network analyzer on a physical device or necessitating the use of computer software:

$$C = \varepsilon_0 l \left[ \left( \frac{w}{d_0} \right) + 0.77 + 1.06 \left( \frac{w}{d_0} \right)^{0.25} + 1.06 \left( \frac{h}{d_0} \right)^{0.5} \right]$$

where $w$ is the width, $h$ is the thickness, $l$ is the overlap length and $d_o$ is the gap. In air $\varepsilon_r$ is equal to 1.

The effects are noticeable. It was calculated before that for $C_{up}$ the value was 44.314fF. Using the above formula gives a $C_{up}$ of 14.32pF, 3.24 times larger than expected. The increase is in line with Chowdhury's estimation.

## 6.3 Incorporating the Actuation Voltage

Three dimensional finite element analysis (FEA) can be used to predict the pull in voltage of a beam structure with very high accuracy. FEA, however, is a very computationally intensive method, and not entirely efficient if the structure is complex [8].

A beam can be designed for a particular actuation voltage. Using the equations presented by Chowdhury for the case of a capacitive switch, we can back solve the physical dimensions of a beam needed to create a switch with almost any actuation voltage.

Understanding the tradeoff between actuation voltage and the initial gap spacing, low actuation switches can be fabricated but at the expense of the up state capacitance. The down state capacitance is also affected by the actuation voltage. The width of the beam determined in the equations directly affects the area of the contacts used to calculate the down state capacitance.

The current drawback of MEMS switches are there high actuation voltages. Without actuation voltages 20V, applications in the digital realm are simply out of the question. Of interest are switches with low actuation voltage. More specifically, low actuation switches that have good RF characteristics.

Silicon dioxide is still by far the most widely used material for MEMS structures. Using $SiO_2$, the dimensions needed to produce capacitive switches with actuation voltages of 20V, 10V, 5V, 3,3V and 1.5V are calculated. The capabilities of current fabrication techniques can be used to easily create switches with these actuation voltages with just a bit of manipulation. The motivation in selecting 5V, 3.3V and 1.5V is to show that voltage issue can be overcome to address digital applications as well.

Table 6-1 shows the physical parameters that will yield particular actuation voltages. As much as possible, the width of the beam was kept as close to 100 μm in order to maintain a square contact area with the 100 μm transmission line width. The thickness and length of the beam are chosen to be 200 nm and 500 μm, respectively. With these three parameters as close to constant as possible, only the air gap will change.

**Table 6-1.** Dimensions for $SiO_2$ beam needed for particular actuation voltages.

| $SiO_2$ | | 20V Design | 10V Design | 5V Design | 3.3V Design | 1.5V Design |
|---|---|---|---|---|---|---|
| Poisson Ratio | v | 0.17 | 0.17 | 0.17 | 0.17 | 0.17 |
| Residual stress | σ (MPa) | 0.1 | 0.1 | 0.1 | 0.1 | 0.1 |
| Young's Modulus | E (GPa) | 75 | 75 | 75 | 75 | 75 |
| Width | w (µm) | 100 | 100 | 100 | 50 | 30 |
| Thickness | t (µm) | 0.2 | 0.2 | 0.2 | 0.2 | 0.1 |
| Length | l (µm) | 500 | 500 | 500 | 500 | 500 |
| Air gap | do | 3.00 | 2.00 | 1.40 | 1.25 | 1.00 |

**Table 6-2.** Down to up state capacitance ratio for each actuation design.

| | 20 V Design | 10V Design | 5V Design | 3.3V Design | 1.5V Design |
|---|---|---|---|---|---|
| $C_{up}$ | 32.7 fF | 47.7 fF | 67.0 fF | 38.8 fF | 29.7 fF |
| $C_{down}$ | 173 pF | 173 pF | 173 pF | 86.3 pF | 51.8 pF |
| **Ratio** | 5281 | 3616 | 2577 | 2223 | 1742 |

The affects of actuation voltage on beam design and in turn RF performance can be seen rather clearly. As the actuation voltage is decreased from 20V to 10V and 5V, only the air gap changes, and in fact, decreases. To obtain the lower actuations of 3.3V and 1.5V the width of the beam must change to keep a reasonable thickness. Nonetheless, the trend exhibited for the higher actuations carry through to the lower actuation voltages. Namely, actuation voltage comes at the expense of the air gap, directly affecting the up state capacitance. Table 6-2 summarizes how much the up state capacitance changes.

We remind the reader that for the RF MEMS switch, insertion loss is governed by the up state capacitance, with lower values being most desirable. Also, the extent of the switch to act ideally off in the off state and on in the on state is given by the ratio of on to off capacitance, or here as down state capacitance to up state capacitance. For the first three cases, $C_{up}$ increases as gap space decreases. The ratio of $C_{up}$ to $C_{down}$ is given as well. As the results show, the quality of the switch to act in an ideal manner degrades substantially as we reduce the actuation voltage. In going from 20V down to 5V, the capacitance ratio decreases half of its starting value. It is harder to see if $C_{up}$ increases or decreases in the lower actuation voltage cases since $C_{down}$ changes, resulting from the different overlap area of the two beam structures. However, looking at the ratios illustrates clearly despite the differences of up and down state capacitance, the switches are overall worse than their higher actuation voltage counterparts.

Another interesting effect is how much the actuation voltage of a beam structure depends on the fabrication process. It turns out that small values of residual stress on the beam structure of the capacitive switch can lead to drastic changes. Table 6-3 shows the values

of actuation voltage with 100KPa of residual stress. This small value was included to mimic the small residual stress in the beam that inherently results from fabrication. This assumed a tightly controlled fabrication process. Despite tight controls on fabrication, residual stresses do occur that can compress or expand the beam. Depending on the extent of stress, the beam can buckle.

If instead the residual stress is 10MPa, 100 times larger than before but still low in a relative sense, the actuation voltages increase wildly. Table 6-3 displays the results for the change in residual stress.

**Table 6-3.** Variation of actuation voltage with a residual stress of 10MPa.

| 20V Design | 10V Design | 5V Design | 3.3V Design | 1.5V Design |
|---|---|---|---|---|
| 67.1V | 41.2V | 27.1V | 18V | 8.23V |

From a design point of view, this large variation cannot be tolerated. One option would be to require tighter controls on fabrication. Another option, in fact an easier option, would be to use a different material. Single crystal silicon could be used in place of silicon dioxide. Single crystal silicon has very little residual stress. If used, the material would null the effects that the fabrication process could potentially introduce. For reference, the dimensions for the beam structures are calculated using single crystal silicon and displayed in Table 6-4. In calculating these new dimensions, a residual stress of 1000Pa is used since the equations cannot support a residual stress of 0. As this factor is 100 times smaller than the 100KPa used previously, the value can essentially be considered 0.

**Table 6-4.** New dimensions using single crystal silicon.

| Single Crystal Silicon | | 20V Design | 10V Design | 5V Design | 3.3V Design | 1.5V Design |
|---|---|---|---|---|---|---|
| Poisson Ratio | v | 0.22 | 0.22 | 0.22 | 0.22 | 0.22 |
| Residual stress | σ (MPa) | 0.001 | 0.001 | 0.001 | 0.001 | 0.001 |
| Young's Modulus | E (GPa) | 150 | 150 | 150 | 150 | 150 |
| Width | w (μm) | 100 | 100 | 100 | 50 | 50 |
| Thickness | t (μm) | 0.2 | 0.2 | 0.2 | 0.2 | 0.1 |
| Length | l (μm) | 500 | 500 | 500 | 500 | 500 |
| Air gap | do | 2.6 | 1.8 | 1.2 | 1 | 1 |

## 6.4 Attenuation

The total RF loss of the switch is the sum of the loss of the structure itself plus the attenuation of the lines. The loss of the lines of the structure, be it return, insertion or isolation, can be found directly from the S-parameters and ABCD matrix.

The attenuation of the line depends on the length of the line itself. The longer the line, the more the signal attenuates. Here, a line length of 500μm is used.

The attenuation must be turned into a decibel loss instead of the constant to which the power of e is raised as is calculated in Frankel. Once expressed in dB, this loss can be added to the loss of the line to give the overall loss of the switch.

Frankel's work shows that the attenuation varies with line dimensions and with frequency. This value is not fixed across all frequency. This work will explore the upper limit on the attenuation over the frequencies of interest to understand the maximum shift of the loss graph, thereby establishing an upper limit on the losses.

To explore how much this loss can be, we calculate the attenuation loss across frequency, from near DC to 100GHz, and as it varies with line dimensions. Presented are the calculations for 5 different line dimensions, for w varied from 0.1μm to 100μm and for s varied from 0.06μm to 60μm. The results are displayed in Table 6-5.

**Table 6-5.** The attenuation in dB of the entire line is shown as it varies with frequency and transmission line geometry. Case 1 has w = 0.1μm and s = 0.06μm; Case 2 has w = 10μm and s = 6μm; Case 3 has w = 30μm and s = 20μm; Case 4 has w = 50μm and s = 30μm; Case 5 has w = 100μm and s = 60μm.

| | Entire Line Attenuation (dB) | | | | |
|---|---|---|---|---|---|
| **f (GHz)** | **Case 1** | **Case 2** | **Case 3** | **Case 4** | **Case 5** |
| **0.01** | 2.43E-13 | 2.43E-13 | 2.43E-13 | 2.43E-13 | 2.43E-13 |
| **0.1** | 2.44E-10 | 2.44E-10 | 2.44E-10 | 2.44E-10 | 2.44E-10 |
| **1** | 2.44E-07 | 2.44E-07 | 2.44E-07 | 2.44E-07 | 2.44E-07 |
| **10** | 0.000 | 0.000 | 0.000 | 0.000 | 0.000 |
| **20** | 0.002 | 0.002 | 0.002 | 0.002 | 0.002 |
| **40** | 0.016 | 0.016 | 0.016 | 0.016 | 0.015 |
| **50** | 0.030 | 0.030 | 0.030 | 0.030 | 0.030 |
| **75** | 0.103 | 0.103 | 0.103 | 0.102 | 0.101 |
| **90** | 0.178 | 0.178 | 0.177 | 0.176 | 0.173 |
| **100** | 0.244 | 0.243 | 0.243 | 0.242 | 0.236 |

The attenuation of the line, regardless of line geometry, has little overall effect on RF loss below 40GHz. Across all geometries, the losses at any frequency are virtually identical. Losses increase with frequency, with the worse loss at 100GHz being just under 0.25dB. Figure 6-1 below shows the line losses for Case 5 which represents the dimensions used in the RF analysis.

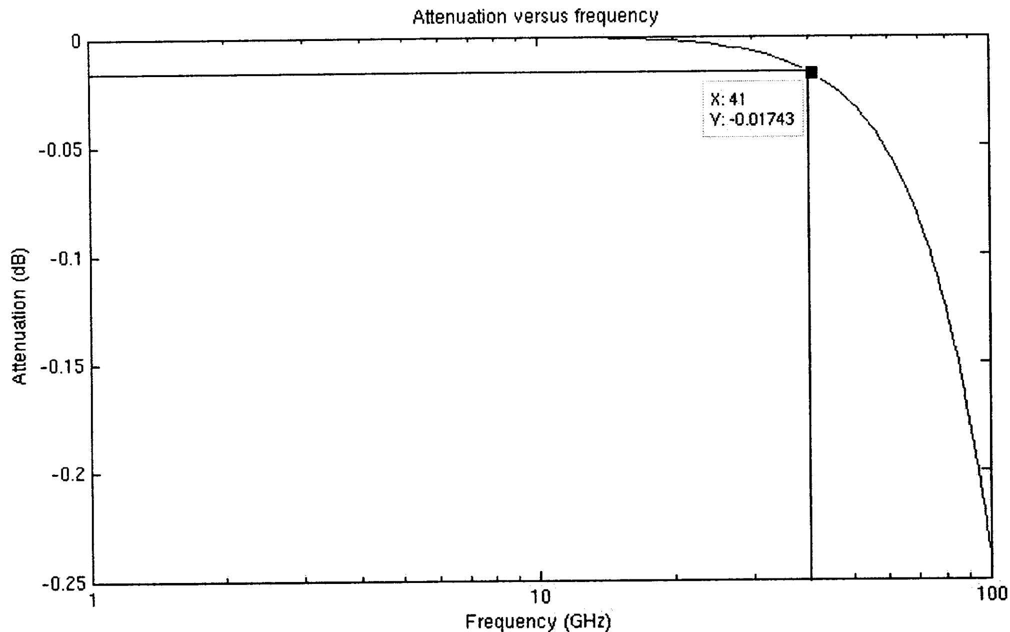


**Figure 6-1**. Line attenuation versus line frequency for line dimensions of w, s and l equal to 100μm, 60μm, and 500μm respectively.

The end result of calculating the line attenuation is that at worst the results obtained from the magnitude plots using S-parameters and ABCD matrix will be .25dB lower. Ultimately, the first TE mode of the device sets an upper limit on the frequency for which these results of this work are valid, namely around 43GHz. From the above figure, the attenuation will be .0175 dB. This value scales linearly with the length of the line. Even if doubled, giving a line length of 1mm, the loss will be .035dB. By way of line lengths, 1mm is very long. Future devices will have lengths much shorter than 500 μm, so the loss from attenuation will be reduced, by a ratio of the length of the smaller line to the 500 μm line for which the loss was originally calculated.

## 6.5 Losses

Calculation of the losses for the capacitive switch was carried out using Matlab. Scripts were written for each type of loss. Losses were first calculated using the dimensions of a switch to yield an actuation voltage of 10V. The length, width, thickness and initial air gap of the beam is 500μm, 100μm, 0.2μm and 2μm, respectively. The coplanar waveguide connected on the input and output side of the switch has a length of 500μm, width of 100μm and a thickness of 0.5μm. Line width to slot ratio was obtained using the synthesis equations. For a width of 100μm, a slot spacing of 59μm is needed to create a 50Ω line at DC. The slot spacing is rounded up to be 60μm for simplicity.

Additionally, losses for switches with dimensions that result in an actuation voltage of 20V and 5V are plotted against the baseline switch. Previously, it was shown how the ratio of down state to up state capacitance decreased as the actuation voltage of the switch decreased. Lower ratios will impact the RF performance. By plotting the losses of these two other switches, the impacts on RF performance can be quantified.

### 6.5.1 Insertion Loss

Insertion loss for the 10V capacitive switch in the up state is displayed in Figure 6-2. From DC up to 10GHz, there is virtually no loss from input to output. Only after 10GHz does the loss begin to deviate from 0dB. The loss becomes increasingly significant. In the decade from 10GHz to 100GHz, the loss drops from 0dB to -3.5dB.

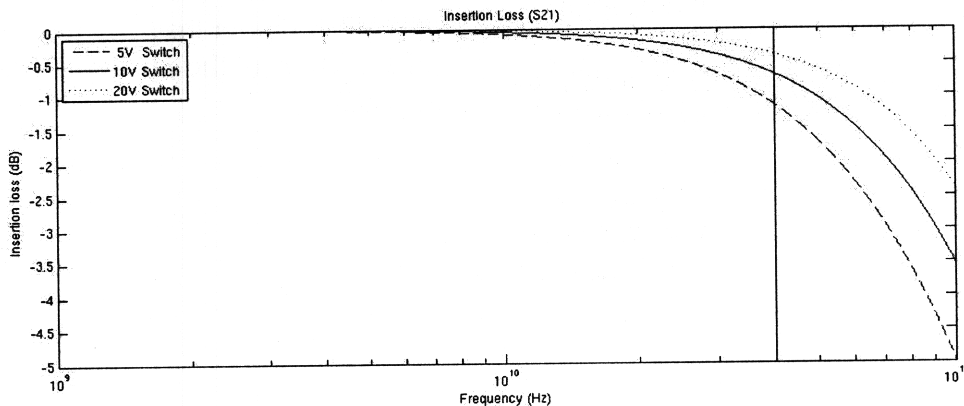


**Figure 6-2.** Insertion loss versus frequency for 5V, 10V, and 20V switch. The vertical line at 40GHz provides a means of comparison for the loss of each switch up to the frequency for which the results are guaranteed.

The insertion losses for the 20V and 5V switch can also be seen. The insertion loss for the 20V switch is plotted as a dotted line and that of the 5V switch as a dashed line. In relation the 10V plot, the plot for the 20V switch is higher, meaning that it experiences less loss than the 10V switch. The dashed line corresponding to the 5V switch is lower than the base line, indicating that there is more loss for this switch. Immediately, it can

be observed just how the capacitive ratio impacts loss. The ratio decreases for decreasing actuation voltage. In the plot this translates to more loss.

Of real interest is what occurs near 40GHz as this is the cutoff frequency for the first order TE mode; after this frequency other modes propagate making the actual results deviate from those found by Matlab. At 40GHz the losses are as follows: -0.39dB for 20V, -0.68dB for 10V and -1.41dB for 5V. If the attenuation is expressed as percentages, at 40GHz the 20V is attenuated 4.4%, the 10V switch 7.5% and 5V switch 15%. Continuing the trend, a switch designed for greater than 20V actuation will experience less than 4.4% attenuation of its input signal while a lower than 5V actuation will experience more than 15%.

The results can be viewed through a different lens. Rather the observing the losses of the data at 40GHz, the data can be used to obtain the bandwidth of tolerable losses for a given switch. In this way design decisions can be made. If, for example, the overall switch cannot attenuation by more than 10% we can use the same figure to find the frequency at which the loss equals -0.5dB, thereby establishing a bandwidth on the frequencies of input signals. As the 5V switch endures the most losses, it should have the lowest bandwidth. Indeed it does. The 5V switch crosses -0.5dB limit at 25.8GHz. The 10V switch is next in line, crossing at 34GHz. The 20V switch has the largest bandwidth. At 4.3.5GHz the 20V switch exceeds the limit. Although 45.3GHz is slightly larger than the cutoff frequency for the first TE mode, the results should conform well to the above plot since the cutoff frequency is just an approximation.

### 6.5.2 Return Loss

Plots for the return loss for each of the three switch types are shown below in Figure 6-3. Unlike the insertion loss case, the plots show little variation between one another, from DC through the highest frequencies of interest. The plots for the return loss look like shifted carbon copies of one another.

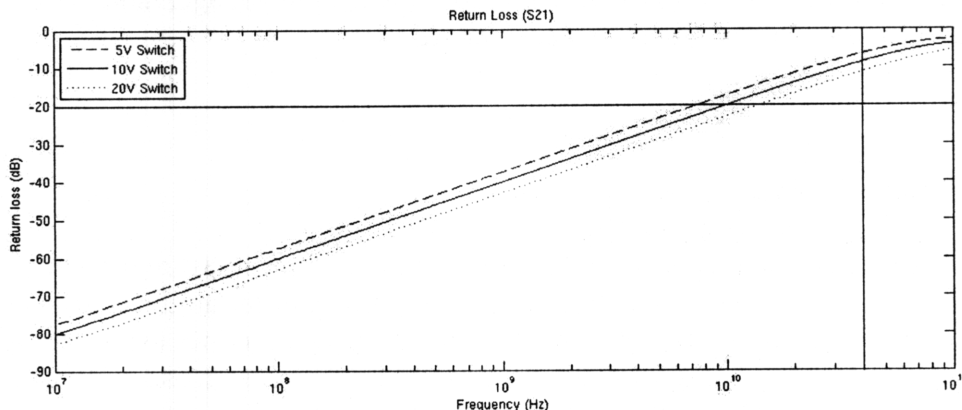


**Figure 6-3**. Return loss versus frequency for 5V, 10V, and 20V switch. The vertical line at 40GHz provides a means of comparison for the loss of each switch up to the frequency for which the results are guaranteed.

An interesting feature shared by all of the plots is that they have linear losses from low to high frequencies. Only close to 100GHz do the plots begin to tail off into what looks like a potential asymptote. If these results were in fact guaranteed this high, we would reach an asymptote. The reason is that the line attenuation means we will always have mismatch.

The plot also suggests that the switches could have better than -80dB return loss at frequencies lower than 10MHz. However, as stated previously, the capacitive switch is not intended to be used for low frequency operation. It is not anticipated return losses will be as low as -80dB. Even if the actual return loss is closer to the value at 1GHz, which is about -45dB, this only represents 0.5% reflection of the input signal back to the source.

At 40GHz the losses for the 20V, 10V and 5V switch are -11.4dB, -8.8dB and -6.6dB respectively. Converting to percents, these are 27%, 36.4% and 46.7%. These losses are very large constituting a tremendous loss on the signal. The small attenuation experienced by the signal as it travels through the switch (7.5%) is offset by the large signal attenuation (36.4%) that results of loading effects for the 10V switch at 40GHz.

Unfortunately, the return loss cannot be improved much more. Considering all practical limitations like air gap, beam dimensions and actuation voltage, the lowest value the up state capacitance can take is 10fF. This value truly might be pushing the bounds of an actual RF MEMS switch since 10fF requires an air gap of 10μm and actuation voltage of 100V. For sake of argument we move forward with this value. At 40GHz, the best return loss that can be obtained is -24dB which is rounded to -20dB for all practical purposes, corresponding to a limit of 10%.

By operating at a lower frequency, the effects of return loss can be reduced. The nature of improving loss at the expense of signal bandwidth is reminiscent of the gain bandwidth product. Taking the same -20dB limit, the bandwidth is 14.2GHz for the 20V switch, 10GHz for the 10V switch and 7.4V for the 5V switch. In order to have a more respectable bandwidth for the switches with lower actuation voltage, more return loss must be tolerated. This is a tough tradeoff indeed.

### 6.5.3 Isolation Loss

The third and last loss of the switch is the isolation loss. In contrast to the insertion and return loss, which both had three plots, there is only one plot for all three switches in Figure 6-4. It is the thickness of the insulating layer that determines the isolation loss in the off state and this is uniform for all of the switches. The design uses a 2nm thin layer which is already using the best fabrication techniques available.

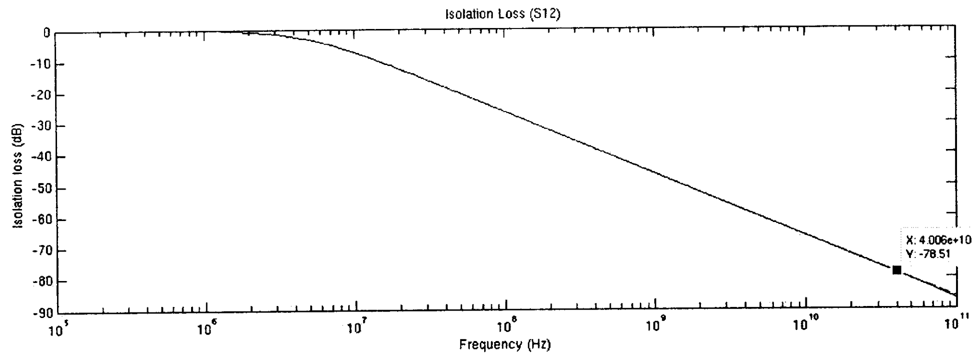


**Figure 6-4**. Isolation loss versus frequency for 5V, 10V, and 20V switch.

The plot itself looks like a mirror image of the return loss. Instead of the loss increasing from low to high frequency, the loss here decreases with increasing frequency. High frequency signals on the output are reflected to a lesser extent on the input than lower frequency signals. Another feature the return and isolation loss share is that they have the same linear behavior. The shape of the plot might be a bit different than the results computed by Matlab, but nonetheless, we expect the same low frequencies behavior of diminishing isolation as the off state capacitance, a shunt capacitor, becomes more of an open circuit. To

As illustrated in the plot, the isolation at 40GHz is -78.5dB. A tighter limit of 1% and 10% can be obtained if the frequencies of signals on the output of the switch are greater than 50Mhz and 500MHz, respectively. This would be ok if one knew what signals to expect to isolate. Most of the harmful voltages that would need to be isolated occur at low frequencies. Any low frequency high voltage event can pass straight through the device and damage circuitry on the input side of the switch. Isolation can be improved by cascading an ohmic switch on the output side, so in effect having two switches to form one overall switch. Yet another option is use the capacitive switch for strictly high frequency applications.

The plot reflects a good upper limit on the isolation loss. Of course, the plot can be changed by increasing the dielectric constant of the insulating material or making the layer thinner altogether. Either serves to increase the capacitance and move the plot down. There are no negative tradeoffs to device performance in increasing the off state capacitance. Tradeoffs show up in device fabrication. Materials required to create high dielectric constants often require more involved deposition techniques or fabrication steps, both which increase the cost in producing the device.

This analysis uses hafnium oxide for the insulating material. It has a dielectric constant of about 30. If a material where used with a dielectric constant of 200, the above plot would move down roughly -10dB. PZT discussed earlier has such a dielectric constant. Unless absolutely needed, high-k materials can be sparred, reducing overall cost yet providing comparable characteristics.

## 6.6 Comparison

Armed with the results from the equivalent circuit models of the capacitive RF MEMS switch what can be said about the future of the device? The simple models presented capture a great deal of the device behavior. With the aim of predicting where RF MEMS switches are going, what insight can be extrapolated from these. Perhaps the question is better rephrased as follows: which characteristics of the RF MEMS switch can be great compared to other switch types and which cannot.

The largest driving factor for the field of RF MEMS switches has been the low RF losses of the device. Academic research has presented devices created with new designs, fabrication techniques, and materials to create devices with better loss values. While losses are a factor, they are not the only factor. Industry needs are for better values for losses while maintaining the low cost, small size, low actuation voltage and long lifetime.

The results of the models presented seem very plausible. The results are supposed to represent an upper limit on device performance. The best comparison found in literature that corroborate the results of this work come from Song in 2006 [11]. In his work, Song reports the measured values for insertion, isolation and return loss of a low actuation voltage capacitive switch from near DC up to 40GHz. At 40GHz, the values for insertion, return and isolation losses for the single capacitive switch are -1.0dB, -12dB dB and -28dB, respectively. For simplicity these results, along with those of the models, are presented below.

**Table 6-6.** Summary of results.

| Losses | This work | Song |
|---|---|---|
| Insertion (dB) | -0.68 | -1 |
| Return (dB) | -78.5 | -12 |
| Isolation (dB) | -8.8 | -28 |

If the results of this work are indeed an upper limit to the measured values of other switches, Song's insertion and isolation loss will be lower while his return loss will be higher. In the table, this is exactly the case. While the insertion loss of -1dB is close to -0.68dB, it is not less than it. The same is true for -28.8dB; it is not less than the limit of -8.8dB. Lastly, Songs return loss of -12dB is less than the -78.5dB required. Around 40GHz, Song results conform to the upper limits obtained from the models very well. Moreover, the fact that Song's insertion loss is close to the upper limit presented indicates devices can approach the limits. More than just a theoretical limit, the values represent a limit that physical switches can approach. Whether the same can be said for return or isolation losses is still unclear.

Actuation voltages presented show that the pull in voltage can be designed to 10V easily with present technology. Obtaining lower actuation voltages is not so much of a challenge with the present state of the art but rather a tradeoff with the more important

RF losses of the switch. Residual stresses play a significant role in varying the observed actuation voltage. For this reason, there should be tight control over the fabrication process, or materials with low residual stresses, like single crystal silicon should be used.

As it stands, the 10V switch was created using a width, length, height, gap distance of 100μm, 500μm, 0.2μm and 2μm, respectively with a Young's modulus of 75GPa and Poisson ratio of 0.17. With the continued development in new materials that have enhanced material properties over those used now, like the lower processing temperatures of poli-SiGe over the more common poli-Si or materials with lower Young's modulus, it seems likely that the same low actuation switches can be made without the need to sacrifice on gap distance, ultimately the limiting factor in RF losses. By increasing the gap distance, switches with low actuation voltages will also have better RF losses, particularly much lower return and isolation losses. Development of new bridge materials will run concurrent with high-k dielectric materials. Improvements in both of these will lead to better devices. Digital applications will benefit directly from these lower actuation voltages. Entry into this sector will create more widespread usage of the RF MEMS switch.

The actuation nature of the RF MEMS switch means they can draw minimal to no power at all. In the capacitive switch, a DC bias is applied to the AC signal of interest. Since there is no DC path to ground, there is no power required to actuate the switch. The same scheme can be employed in the ohmic switch.

Power handling is still a matter better left to other switching technologies. Ideally, in an industry like ATE where hot switching events do occur, an RF MEMS switch should be able to tolerate these spurious occurrences without failing. Hot switching substantially decreases the lifetime of a switch. Referring the SPST switch by Radant MEMS in [51], increasing the hot switched power from -10dBm (100μW) to 20dBm (100mW), leads to a decrease in lifetime from $10^9$ to $10^3$ cycles. Alternatively, an increase in switched power of 1000 leads to a decrease in lifetime of 1,000,000. Some RF MEMS relays that have been developed for the automotive industry can handle switching large currents. Work by Qui [55] can switch currents up to 3A at a rate of 5Hz. High power devices like the latter are generally larger in size, slower in actuating and have lower lifetimes than the switch explored in this work.

The on resistance a parameter only specific to the ohmic contact switch. Switches have been made to have on resistances in the tens of milliohms range. Ultimately, it is not so much low resistances that are important for ohmic contact switches, but the time over which the resistance stays stable without too much fluctuation. By way of example, a switch with an on resistance of 1Ω over 100 million actuations would be more desirable than a switch having a resistance of 10mΩ that is stable over 100 thousand actuations. The work found in academic literature and from the commercial sector like Omron suggest that 1Ω and less will be the typical on state resistance of ohmic switches.

Compared to other parameters, switching time seems to have taken a back seat role. The needs of RF MEMS switches, particularly with the focus of the automated test industry,

have been at present geared towards linearity, power, pull in voltage and stability in contact resistance. Fast actuating switches can be produced, but these come at the expense of the other parameters that have become of interest. For instance, increasing the actuation voltage of the device, increases the contact force, and causes the switch to close faster. However, higher contact forces lead to the degradation of the lifetime of the switch. Goldsmith showed that for every 5-7V decrease in actuation voltage, the lifetime of a capacitive switch increases an order of magnitude [45]. The limits of actuation speed are hard to predict at present seeing as they are contingent on other characteristics and not a priority. Based on the progress of switches and where work on mechanics and the dynamic behavior of the switches themselves, it is possible that speeds around 1μs will be the norm in future switches.

All of these factors in mind, Table 6-7 summarizes the results of the RF MEMS switch compared to PIN diodes, optoFets and semiconductor switches as was done in Table 2-1. Formal comparison across each parameter shows the strengths and weaknesses of each switch type. PIN diodes, for instance, have low actuation voltage but high on resistance. An additional benefit of Table 6-7 is that it can serve as a lookup table for a designer in search of a suitable switch.

**Table 6-7.** Modified summary of important characteristics for different switch types.

| **Parameter** | **MEMS** | **PIN Diode** | **OptoFET** | **Semiconductor** |
|---|---|---|---|---|
| **Voltage (V)** | 10 | 0 - 5 | 1.1 – 3.5 | 0.5 – 5 |
| **Current (mA)** | 50 | 3 - 20 | 1 – 5 | 0.02 – 3 |
| **$R_{on}$ (Ω)** | <1 | 10k | 0.75 – 10.5 | 50 |
| **Power Consumption** | 0 | 5 - 100mW | 0.4 - 1 W | 0.05 – 15mW |
| **Power Handling (W)** | | | | |
| **Cold Switching** | 0 – 4 | 0.1 – 1 | 0.15 – 0.9 | 0.25 – 2 |
| **Hot Switching** | 0 – 4 | 0.05 – 0.5 | 4 – 24 | 0.15 -1.3 |
| **Switching Speed (μs)** | 1 | 1.5 | 100 – 400 | 0.01 - 2 |
| **Freq. Range (GHz)** | DC – 40 | 0.5 - 8 | DC – 100 | DC – 5 |
| **Return Loss (dB)** | 78.5 | 11 | None | 20 |
| **Insertion Loss** | 0.68 | 3 | None | 1.5 |
| **Isolation Loss** | 8.8 | | None | 40 |

Using a ranking system of low, medium, high, fast and slow, the same information in Table 6-7 can be conveyed but in a slightly different form. Comparison across the switch types is made easier by abstracting away the numerical values of each parameter.

**Table 6-8.** Comparison of the important characteristics for different switch types.

| Parameter | MEMS | PIN Diode | OptoFET | Semiconductor |
|---|---|---|---|---|
| **Voltage (V)** | Hi | Low | Low | Low |
| **Current (mA)** | Hi | Medium | Low | Low |
| **$R_{on}$ (Ω)** | Low | Hi | Medium | Hi |
| **Power Consumption** | Low | Medium | Hi | Low |
| **Power Handling (W)** | Low | Medium | Hi | Medium |
| **Switching Speed (μs)** | Fast | Fast | Slow | Fast |
| **Freq. Range (GHz)** | Hi | Low | Hi | Low |
| **Return Loss (dB)** | Low | Hi | None | Low |
| **Insertion Loss** | Low | Hi | None | Medium |
| **Isolation Loss** | Medium | Low | None | Hi |

Based on RF characteristics alone, Table 6-8 shows RF MEMS switches represent the best technology to use. The low return loss, low insertion loss and medium isolation loss make the switch very enticing. Over the range of DC to 40GHz, the RF MEMS capacitive switch performs very well. RF MEMS switches are most suited for applications that require low RF losses and small size. For other applications where different characteristics are also a priority, careful consideration must be given to the use of an RF MEMS switch.

Despite the great RF performance of the capacitive RF MEMS switch, the device is an endeavor only pursued in the academic realm; there are no capacitive MEMS switches on the market to date. Interestingly, the RF MEMS switch that has had the most success in the commercial market is actually an ohmic switch produced by Radant MEMS. Radant MEMS is one of the few companies that has not gone bankrupt in the development or production of commercial RF MEMS. Their first commercial product was a cantilever structure capable of operation up to 10GHz with an insertion, isolation and return loss of 0.32dB, 12dB and 20dB. Subsequent devices have incorporated multiple poles and multiple throws. Noted previously was the fact that ohmic switches are not suited for high frequency operation because of the poor losses they have compared to their capacitive counterpart. As the devices are ohmic switches, the values reported by Radant cannot be directly compared to the results of the capacitive switch. It is sufficient to say, however, that the RF losses are worse than those of the capacitive switch, even though the ohmic switches can be used in the gigahertz regime.

MEMS technology is one of reducing the size of devices. Many individual devices can be made to fit within the same footprint of a solid state device. As a result, one trend will be the matrix configuration of multiple MEMS devices. The release of the single pole four throw and single pole six throw switch by Radant highlights this trend [52],[53]. Expect to see devices with multiple poles and multiple throws. As long as the issues of reliability along with low cost can be met, expect this device to become of high interest to the field of automated test equipment, where board real estate is always at a premium.

# Chapter 7

# Packaging

Lately, the field of packaging has become a hot topic. Although packaging of MEMS devices has always been important, it has evolved into more than just device protection within the past few years. For the field of RF MEMS switches, packaging has needed to address a number of other issues instead of just device protection including:

- Packaging method
- Packaging materials (ceramic, metal, glass)
- Operational environment (hermetic vacuum or direct exposure)
- Die placement in package
- Wire bonding and sealing
- Bonding technologies
- Cleanliness of packaging area
- Standards

The list begins to describe the various areas and challenges in packaging a MEMS switch commensurate to the factors that lead to a good design. In as much detail as it relates to the electrical characteristics of a MEMS switch, these distinct categories are discussed.

## 7.1 Packaging Methods

The packaging of RF MEMS switches can be separated into two classes, wafer bonding and wafer level packaging. Wafer bonding, also called 1-level, uses a cavity lid to package a device. The former class of device packaging is known as wafer level micropackaging or 0-level packaging. Instead of bonding a separate wafer or cavity to the fabricated MEMS devices, micropackaging encapsulates devices individually on the wafer. These structures are deposited as part of the fabrication process.

A typical 0-level package process flow is as follows, illustrated in Figure 7-1. First a sacrificial layer is deposited on top of the MEMS device. Another layer is then deposited on the sacrificial layer. An etching process is then used to remove the sacrificial material that covered the device, thereby releasing the MEMS structure. To assist in the etching process, holes are left in the layer that serves as the package to enhance the etching process that removes the sacrificial layer. Although more holes increases the etch rate,

there is a tradeoff between time and the mechanical integrity of this layer. Porous materials have also been used [24]. The last step is to cover the etch holes in order to isolate the device from the outside environment.

Even though wafer level packaging can be done before or after the wafer is cut into die (where the devices are separated individually), the preference goes to applying wafer level packaging before the cutting process. MEMS devices are easily damaged when the wafer is sawed to cut into dies. Performing 0-level packaging before the release of the MEMS device ensures that the device will not be mechanically damaged during the separation process while at the same time simplifying back end processing, reducing costs [25], and providing a contamination free surface [26].

Wafer level packaging is effective for small volume production because it makes batch assembly possible. It also eliminates the need for automated machines as part of the assembling process for each chip [7]. Often, as part of the release process, a self assembled monolayer (SAM) coating is applied to MEMS to reduce stiction induced by moisture.

1-level packaging is slightly different. Instead of the devices being packaged at the wafer level, the device wafer is cut into die that are then placed into packages by standard die attach techniques. It is more expensive than 0-level since it must satisfy the environmental requirements for the final product, but in turn provides the ultimate environmental protection than 0-level. 1-level packaging is done with a ceramic or metal with a solder sealed lid. While wafer bonding draws from the benefits of using IC packaging technologies that have been tested and proven, the main drawback to this method is the inclusion of a seal ring needed to complete the bond between the device and its enclosure. The seal ring adds unwanted parasitics, increases device area (chip real estate) and signal loss.

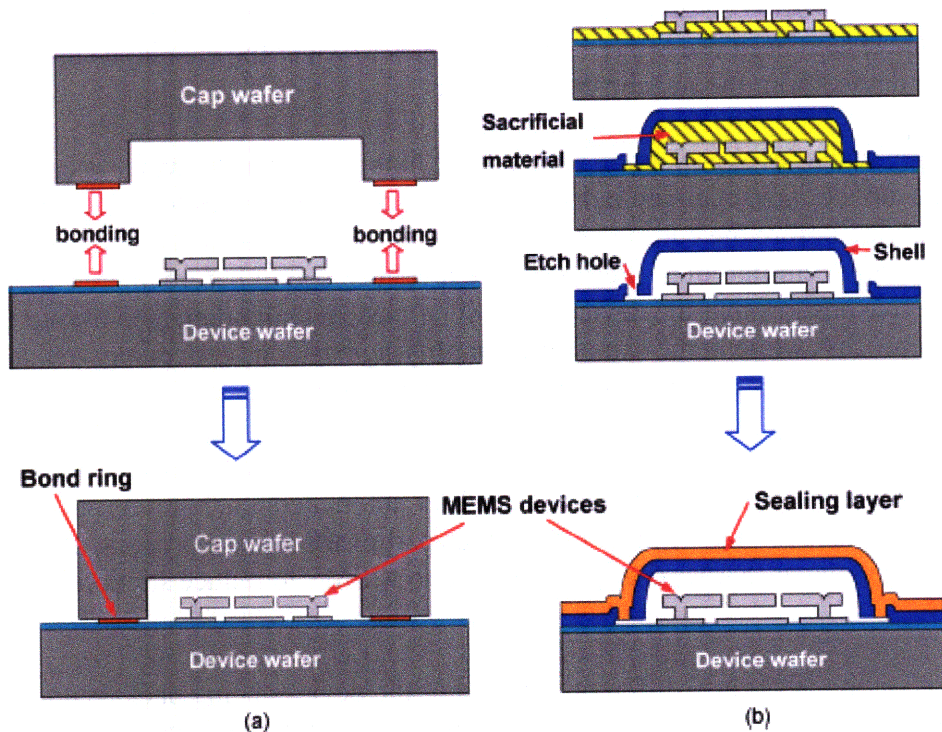


**Figure 7-1.** Illustration of (a) wafer bonding and (b) wafer level packaging.

## 7.2 Packaging Materials

The two most commonly used materials to encapsulate MEMS structures are silicon or glass. For glass, electrical connections are maintained by electrical feedthroughs. Getters are used to absorb residual moisture. In addition to a hermetic seal, this type of package offers superb reliability as the contact surfaces are kept clean from contamination. This type of packaging has been used by Advantest Corporation [7].

Metals can also be used. Metal packages are typically constructed of Kovar with glass bead passthroughs. When different materials are used in conjunction with one another, cracking becomes a concern. To prevent this, the Kovar and glass have matched coefficients of thermal expansion. In some cases the use of ceramic is desirable. Aluminum oxide also called alumina most often used material. If high thermal conductivity is required, beryllium oxide (beryllia) used, but it is toxic; aluminum nitride can be used in place.

## 7.3 Die Placement in Package

Devices that are not packaged at wafer level present challenges in packaging at the die level, once they are cut. MEMS devices are sensitive to any form of mechanical stress and contamination. Small residual stresses in the capacitive switch lead to wild variations in actuation voltage. Forces on the order of mN are sufficient to damage small

parts. Even the smallest of particles can short connections or prevent actuation. Unless careful measures are taken, problems arise. This is precisely the concern with the vacuum handling used by integrated circuits. This automated packaging process uses a probe that suctions to the top surface of the device to move it into a package. Any missteps in applied force or environment can render parts useless. Although techniques that have been shown to work with ICs, these do not necessarily carryover to MEMS.

Implemented correctly and with caution, vacuums can be used. To reduce the chance of mechanical damage, the tip that contacts the device can be set to touch an unimportant area of die. To mitigate the chance of small holding forces and concentrated loads due to the application of the tip, Sandia National Labs uses a handling tool with a recessed center and vacuum on edges to grab devices without damaging them.

Once the device is placed it must be secured in the package. Oven cured epoxies are used to fasten the MEMS device in place. This simple step has its share complexities. Short curing times require high temperatures (15 min @175°C) and low temperatures require longer times (60 min @150°C). The benefit of low temperature is that is preserves any coating applied to MEMS device. Higher temperatures serve to drive out more of the volatile gasses from the epoxy thereby reducing contamination. Moreover, there is a sweet spot in this time and temperature profile that makes finding the optimal spot a matter of experimentation. The times and temperatures depend on manufacturer or consumer needs.

## 7.4 Wire Bonding and Sealing

Typical RF substrates only allow conductive traces on top or bottom. From an RF design standpoint, wires have parasitic inductances, and the need to reduced unwanted parasitics means that connections should be kept as short as possible. Stacking circuits one of top of the other would reduce wire length substantially. Co-fired ceramics allow ceramic material layers to be stacked with conductive traces sandwiched between each layer. Devices using co-fired ceramics have been stacked up to 50 layers, reducing component count and interconnection length. These ceramics are temperature treated materials. Since materials shrink when treated, resulting from the coefficient of thermal expansion, it is difficult to design circuits across various layers.

Wire bonding connections to devices is standard for integrated circuit devices. To connect conductive traces from the device to the package in which it is housed, wires are bonded to the traces using solder. Wire bonding posses two problems. Matched impedances are important for high fidelity RF characteristics in MEMS switches. Differences in the impedance of the solder to the bond bad cause unwanted reflections. Using wire-bond wires it is hard to construct balanced transmissions as they add parasitics due to length. The resistance of the thin wires can be high enough to create significant losses in the circuit. One solution for a large number of interconnect is to use gold plated copper ribbons. Numerous ribbons can handle high current, but at the expense of high parasitic inductance. Thus, we see again that although MEMS

technology leverages a number of proven processes and fabrication from the IC realm, there are important issues that must be addressed aside from MEMS design to create a high fidelity device.

Flip chip and tape automated bonding (TAB) are also used to form connections. The conductivity of these methods, though, is not good enough for good RF performance.

## 7.5 Bonding Technologies

Bonding is done by standard IC packaging methods such as fusion bonding, anodic bonding, eutectic bonding, thermocompression bonding or epoxy bonding. Where one bonding type would be good for a particular application, the same might not be for another. Below is a quick description of the various types mentioned.

Fusion bonding is a commonly used manner of bonding together two silicon wafers. The process requires high temperatures (>800°C), an oxidizing environment, and low surface roughness to ensure a good bond. The strong bond that results is due to the chemical reaction of the OH groups on the surface of the silicon [25].

Anodic bonding is the bonding of a silicon wafer with a glass wafer. Each of these materials can serve as the substrate or the package of the RF MEMS switch. By applying a two step process of high heat (180°C to 500°C) and voltage (200-1000V), a very strong and irreversible silicon-oxide bond is formed. The environment inside the device can be a vacuum, dry air or inert gasses, ultimately dependent on the requirements of the device.

Eutectic bonding is a process in which wafers of different materials can be bonded together. To bond these materials, pressure is used to 'glue' them. The bond is usually created using a Au-Si glue but can also be formed using Au-In or Au-Sn. First, an Au seal ring is patterned on the silicon device. Then the wafers are brought together. With an applied mechanical pressure, the Au and Si turn into a solution. As the temperature is raised the solution stops melting (~375°C).

The technique of simultaneous application of pressure and temperature is known as thermocompression. Like eutectic bonding, thermocompression can bond any two wafers together via a bonding material at the wafer interface, typically a gold thin film. The bonding method relies on the formation of metallic bonds by means of diffusion. Normally, when two materials are brought together at room temperature high pressures are needed. If the temperature is raised, the pressure can be lowered. While any material can be bonded together, the requirements on pressure and temperature might not be suitable for particular applications [27].

Epoxy bonding leverages the same process as eutectic bonding. The difference between packaging methods is the type of 'glue' used. Conductive epoxies are often used in place of a eutectic die bond. While being less electrically efficient and even less efficient mechanically and thermally, epoxy bonding is implemented as it is a more robust

packaging method that is very tolerant to process variation [28]. Processing temperatures for epoxies are less than 150°C making them much lower than eutectic bonding. Epoxies occasionally experience out-gassing during or after curing that could contaminate the device leading to reliability problems. Low out-gassing epoxies, however, have been designed to address this problem, making it suitable to employ epoxies for some types of switches.

## 7.6 Standards

While people recognize the need to package devices well, there are no governing standards in place for field of MEMS as there are in the field of integrated circuits. The absence of standards has made the issues of low costs, materials and packaging type, issues directly affecting the adoption of MEMS into the commercial realm, difficult to address. On the whole, however, there is a lot of work being done in regards to addressing standards.

Currently, there are no adopted industry standards for packaging as there are in the integrated circuit industry. MEMS packaging largely remains application specific and proprietary information to the companies or universities that produce them. Some standards have come from the military sector [29] that pertain to cleanliness and hermeticity. Research is trying to get closer to these ideals while making it cost effective. There are a number of groups working on refining packaging, researching the current state of the industry, and providing new packaging technologies for the RF MEMS field. Among key players have been Sandia National Labs, the University of Arkansas, and WiSpry Incorporated [30]. Recent figures show that the packaging costs of RF MEMS devices can reach up to 70% of the total cost [31] owing to the special techniques and materials that must be used. Lastly, different packaging technologies yield different device performance.

RF MEMS requirements are much different, and in fact more rigid, than normal MEMS devices, as the packaging for RF MEMS must minimize the attenuation of high frequency signals. No thresholds exist to denote acceptable values for insertion, isolation or return loss after which diminishing marginal returns of cost to performance can be assessed. Instead, characteristics are optimized subjectively by discretion.

While the field of RF MEMS is rather well established, in terms of processing, models, theory, and device types, the field of standards is not nearly where it needs to be for switches to become alternatives to present solid state of mechanical switching technology where cost is a priority. The successful adoption of RF MEMS switches will depend on defining packing standards across the industry [32].

## 7.7 Operational Environment

In addition to creating a high fidelity device, its integrity must be preserved in various environments and conditions. Packaging must protect the device without altering its performance. And there exists so much more beyond selecting a package to protect the device. Considerations include humidity, hermicity, temperature, contamination, process compatibility, etc. Eventually, since mechanical parts and components are often temperature sensitive, packaging will need to move to low process temperatures [31].

Humidity is perhaps the largest factor affecting performance. Goldsmith's work on the lifetime characterization of an RF MEMS switch reveals that ambient humidities greater than 30% in open air leads to stiction. [45]. To prevent stiction of this sort, removal of all humidity is desirable. Dehydrations bakes are used, followed by a hermetic seal, seal of dry gas, and getters to ensure a long lasting seal.

## 7.8 Wafer Level Packaging

Results of packaging type on losses were taken from the fabrication and testing of MEMS phase shifters [31]. Figure 7-2 displays the result that the observed losses depend on the packaging used. For the case of insertion loss, values should be as close as close to 0dB as possible. For return loss, large negative values are desirable. The results indicate that wafer level micropackaging is best in both cases.

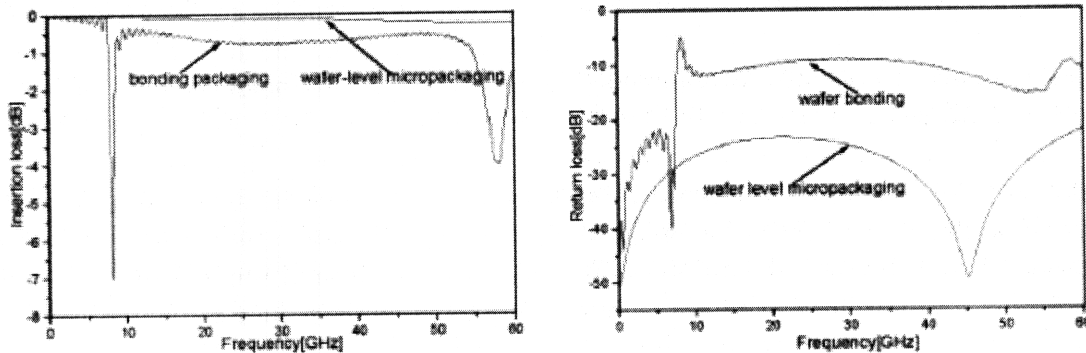


**Figure 7-2**. Differences in electrical characteristics based on packaging modes.

Some RF MEMS switch packaging information postulated in this work comes from work in other areas of MEMS. For example, a MEMS resonator has been packaged in a vacuum chamber buried under a wafer surface using polysilicon [33]. Due to negligible gas absorption, long term drift is less than 1ppm. The stacked circuit chip design of the device means that drift due to temperature from -40°C to +85°C is less than 100 parts per billion. From these results that the characteristics of an RF MEMS switch designed and packaged in this fashion can potentially be very well preserved.

# Chapter 8

# Summary and Conclusion

## 8.1 Summary

To understand what MEMS technology is and how it can be used to create a switch, this thesis starts off with an introduction (Chapter 1). The background in Chapter 2 serves to to bring the reader up to a good level of understanding of the different switch structures, viable use at radio frequency and the issues affecting reliability. Typical values (Section 2.4) are also presented to give the reader a flavor of the characteristics of a switch. The two main structures are the cantilever and beam.

As much as the switch is an electrical device, it is also a mechanical one. Analysis for the operation and characterization of the RF MEMS switch begins by modeling the mechanics of these structures (Chapter 3). With formulas relating the dimensions and dynamics of the device to actuation voltage and capacitance, the RF performance can be investigated.

The RF losses of the switch are calculated using the electrical modeling of Chapter 4. Sections 4.1 and 4.2 present a first order model of the capacitive and ohmic switch. The capacitive switch has a capacitor that separates input to output in both the on and off state. The ohmic switch has a capacitor in the off state and a resistor from input to output in the on state. Section 4.3 presents some of the parasitic elements that change the first order model and actually better describe the observed behavior of the switch. Although there are parasitics for the capacitive switch, most of the device operation is described well by using just a capacitor (Section 4.3.1). Scaling the values of prior work [55], the parasitic resistance and inductance that affect RF performance of the ohmic switch can be approximated (Section 4.3.2).

Electrical modeling of the frequency effects of transmission lines (Section 4.4) is also considered. Transmission lines serve the function of electrically connecting a signal from the outside of a package to the switch itself. These connections contribute to the RF losses of the switch. For the capacitive switch, the coplanar waveguide structure in Figure 4-9 has frequency dependent losses determined by the effective characteristic impedance of the line ($Z_{cpw}$ page 29) and an attenuation per unit length of the line ($\alpha_{cpw}$ page 30). Section 4.4.4 describes how a line can be designed to obtain a particular characteristic impedance, such as the 50Ω or 75Ω common to RF applications.

The result of the mechanical and electrical modeling is the formation of a complete device model (Section 4.7). The RF losses, insertion, isolation and return loss, are calculated from this complete device model using S-parameters (Section 4.6) and the ABCD matrices (Section 4.7.3). Finally, the losses are used to compare RF MEMS switches to other switching technology (Section 6.6) and predict values of future RF devices.

Current work (Chapter 5) within the field of MEMS switches aims to understand and explain issues of contact resistance (Section 5.1) and stiction (Section 5.2). New switch designs (Section 5.3), overall system integration (Section 5.4), materials (Section 5.5) and fabrication techniques (Section 5.7) switches. Coupled with advances in device packaging methods and standards (Section 7.1 and 7.6), the current work will continue to contribute to the creation of better devices.

## 8.2 Conclusion

There are a number of lessons learned throughout the course of this survey and analysis on RF MEMS switches. The first and foremost is that there is no single great switch. There are always tradeoffs and drawbacks to any switch technology. MEMS switches are no exception to this paradigm. Although RF MEMS switches have great values for RF losses, they have slow actuation times, some issues with lifetime, and are not meant to switch high loads. Work on stiction (Section 5.2) and continued research on the power handling capabilities of the device suggests that these values will become better.

From an industry perspective, another deterrent to widespread adoption of RF MEMS switches is not the issues of reliability but the high cost of the device. Bought on a per unit basis, the Radant MEMS SPST switch costs $20. While RF MEMS switches have good characteristics, there is no sound argument from a cost perspective to pay 2, 5, or even 10 times more for a MEMS switch which provides only marginal improvements over a cheaper semiconductor switch. The cost of this commodity will fall once they become technically successful. Once this does, more attention will be given to the RF MEMS switch.

Overall adoption will be based on the technical merits of the switch. The RF losses of the capacitive switch (Section 6.5 and Table 6-7) are low and in fact better than the other switching technologies used for RF applications. These will only continue to be better with development of higher dielectric constant materials like PZT and will lead to better RF losses.

# Chapter 9

# Matlab Code

Below are the Matlab scripts used to calculate the insertion, return and isolation loss of the switch. As it stands, since they are functions, these can be copied directly over into an M file and run as is.

## 9.1 Insertion Loss

```
function loss = ins(f)

%RF Characteristics of Capacitive switch with transmission lines

%LINE VALUES for a nominal 50 Ohm line, which will change as frequency
increases
      w = 100e-6;
      s =  60e-6;
      l = 500e-6;
      t = 0.5e-6;

%BEAM VALUES for 10V
       w_b = 100e-6;
       l_b = 500e-6;
       t_b = 0.2e-6;
       g   =   2e-6;
       h   = 525e-6;

% Calculate Cup
      c     = 3e8;
      er    = 11.7;
      pi    = 3.14159;
      eo    = 8.85419e-12;
      Cup   = eo*l*(  w_b/g + 0.77 + 1.06*(w_b/g)^(0.25)
      +1.06*(h/g)^(0.5) );

% Calculate eff
      eq   = (er+1)/2;
      q    = log10(w/h);
      v    = 0.43-0.86*q+0.54*q^2;
      u    = 0.54-0.64*q+0.015*q^2;
      a    = 10^(u*log10(w/s)+v);
      f_te = c/(4*h*sqrt(er-1));
```

```
      k  = w/(w+2*s);
      kp = sqrt(1-k^2);
      K  = ellipke(k^2);
      Kp = ellipke(kp^2);

eff_f = ( sqrt(eq) +  (sqrt(er) -sqrt(eq))./(1.+a.*(f./f_te).^(-1.8))
).^2 ;

Z_f   =  120.*pi./(4.*sqrt(eff_f)).*(Kp)./(K);

a_f  =  (pi./2).^5 .* 2.* ((1-eff_f./er).^2 ./ sqrt(eff_f./er)) .*
(w+2.*s).^2.*er.^(3./2)./(c.^3 .* K.*Kp) .*f.^3;

b_f  =  2.*pi.*f./c.*sqrt(eff_f);

%a_f is per m, want to find in dB

afdb =20*log10( exp(-2*a_f*l));


% Need to add in S-parameters
       Y_f = 1./Z_f;
       b_fl=b_f.*l;

       A = cos(b_fl);
       B = j.*Z_f.*sin(b_fl);
       C = j.*Y_f.*sin(b_fl);
       D = A;
       Yu = j.*2.*pi.*f.*Cup;


% Insertion Parameters
& One could multiply the three matrices together as mentioned in
% Y.7.3     (ABCD matrix and losses)
% For simplicity the author shows the calculation resulting from the
matrix multiplication

Au = A.*(A+B.*Yu) + B.*C;
Bu = B.*(A+B.*Yu) + B.*D;
Cu = A.*(C+D.*Yu) + C.*D;
Du = B.*(C+D.*Yu) + D.*D;

% INSERTION Loss
      S21 = 2./(Au+Bu./Z_f+Cu.*Z_f+Du);
      magS21 = sqrt(real(S21).^2+ imag(S21).^2);
      loss = 20*log10(magS21) + afdb;
```

## 9.2 Return Loss

```
function loss = ret(f)

%LINE VALUES for a nominal 50 Ohm line, which will change as frequency
increases
      w = 100e-6;
      s =  60e-6;
      l = 500e-6;
      t = 0.5e-6;

%BEAM VALUES for 10V
      w_b = 100e-6;
      l_b = 500e-6;
      t_b = 0.2e-6;
      g   =   2e-6;
      h     = 525e-6;

% Calculate Cup
      c=3e8;
      er    = 11.7;
      pi    = 3.14159;
      eo    = 8.85419e-12;
      Cup   = eo*w*(  w_b/g + 0.77 + 1.06*(w_b/g)^(0.25)
      +1.06*(h/g)^(0.5)  );


%Calculate eff
      eq   = (er+1)/2;
      q    = log10(w/h);
      v    = 0.43-0.86*q+0.54*q^2;
      u    = 0.54-0.64*q+0.015*q^2;
      a    = 10^(u*log10(w/s)+v);
      f_te = c/(4*h*sqrt(er-1));

      k  = w/(w+2*s);
      kp = sqrt(1-k^2);
      K  = ellipke(k^2);
      Kp = ellipke(kp^2);

eff_f = ( sqrt(eq) +  (sqrt(er) -sqrt(eq))./(1.+a.*(f./f_te).^(-1.8))
).^2;

Z_f   =  120.*pi./(4.*sqrt(eff_f)).*(Kp)./(K);

a_f  =  (pi./2).^5 .* 2.* ((1-eff_f./er).^2  ./ sqrt(eff_f./er)) .*
(w+2.*s).^2.*er.^(3/2)./(c.^3 .* K.*Kp)  .*f.^3;

b_f  =  2.*pi.*f./c.*sqrt(eff_f);

% a_f is per m, want to find in dB
      afdb =20*log10( exp(-2*a_f*l))
```

```
% Add in S-parameters
       Y_f = 1./Z_f;
       b_fl=b_f.*l;

       A = cos(b_fl);
       B = j.*Z_f.*sin(b_fl);
       C = j.*Y_f.*sin(b_fl);
       D = A;
       Yu = j.*2.*pi.*f.*Cup;


% ABCD Matrix Parameters
      Au = A.*(A+B.*Yu) + B.*C;
      Bu = B.*(A+B.*Yu) + B.*D;
      Cu = A.*(C+D.*Yu) + C.*D;
      Du = B.*(C+D.*Yu) + D.*D;


%RETURN Loss
      S11 = (Au+Bu./Z_f-Cu.*Z_f-Du)./(Au+Bu./Z_f+Cu.*Z_f+Du);
      magS11 = sqrt(real(S11).^2+ imag(S11).^2);
      loss = 20*log10(magS11) + afdb;
```

## 9.3 Isolation Loss

```
function loss = iso(f)


%LINE VALUES for a nominal 50 Ohm line, which will change as frequency
increases
      w = 100e-6;
      s =  60e-6;
      l = 500e-6;
      t = 0.5e-6;

%BEAM VALUES for 10V
      w_b = 100e-6;
      l_b = 500e-6;
      t_b = 0.2e-6;
      g   =   2e-6;
      h     = 525e-6;

% Cdown
      Cdown = 4.33*10^-9;

%Calculate eff
      eq    = (er+1)/2;
      q     = log10(w/h);
      v     = 0.43-0.86*q+0.54*q^2;
      u     = 0.54-0.64*q+0.015*q^2;
      a     = 10^(u*log10(w/s)+v);
      f_te = c/(4*h*sqrt(er-1));

      k  = w/(w+2*s);
      kp = sqrt(1-k^2);
      K  = ellipke(k^2);
      Kp = ellipke(kp^2);

eff_f = ( sqrt(eq) +  (sqrt(er) -sqrt(eq))./(1.+a.*(f./f_te).^(-1.8))
).^2;

Z_f   =  120.*pi./(4.*sqrt(eff_f)).*(Kp)./(K);

a_f  =  (pi./2).^5 .* 2.* ((1-eff_f./er).^2 ./ sqrt(eff_f./er)) .*
(w+2.*s).^2.*er.^(3./2)./(c.^3 .* K.*Kp)  .*f.^3;

b_f  =  2.*pi.*f./c.*sqrt(eff_f);

%a_f is per m, want to find in dB
      afdb =20*log10( exp(-2*a_f*l))

% Need to add in S-parameters
       Y_f = 1./Z_f;
       b_fl=b_f.*l;

       A = cos(b_fl);
       B = j.*Z_f.*sin(b_fl);
```

```
        C = j.*Y_f.*sin(b_fl);
        D = A;
        Yd = j.*2.*pi.*f.*Cdown;

% ABCD  Matrix Parameters
       Ad = A.*(A+B.*Yd) + B.*C;
       Bd = B.*(A+B.*Yd) + B.*D;
       Cd = A.*(C+D.*Yd) + C.*D;
       Dd = B.*(C+D.*Yd) + D.*D;

%ISOLATION Loss
       S12 = 2.*(Ad.*Dd-Bd.*Cd)./(Ad+Bd./Z_f+Cd.*Z_f+Dd);
       magS12 = sqrt(real(S12).^2+ imag(S12).^2);
       loss = 20*log10(magS12)+ afdb;
```

# Bibliography


1 L.E. Larson, R.H. Hackette, and R.F. Lohr, "Microactuators for GaAs-based microwave integrated circuits," Transducers'91 Int. Conf. Solid-State Sens. Actuators Dig., pp.743–746, June 1991

2 Bouchaud, Jérémie and Knoblich, Bernardo, RF MEMS Switches Deliver on Early Promise, Wicht Technologie Consulting (WTC), October 16, 2007, http://internetcommunications.tmcnet.com/topics/broadband-mobile/articles/12581-rf-mems-switches-deliver-early-promise.htm

3 S. Pamidighantam et. al, Pull-in voltage analysis of eletrostatically actuated beam structures with fixed-fixed and fixed-free end conditions, J. Micromech. Microeng. '02 Vol. **12** 458-464

4 J. Wong, An electrostatically actuated MEMS switch for power applications, JMEMS, 2000 633-638

5 J. Lee, A low-loss single-pole six-throw switch based on compact RF MEMS switches, IEEE Trans. Micro. Theory and Tech. Vol. 53 No. 11 2005, 3335-3344

6 J Robertson, High dielectric constant gate oxides for metal oxide Si transistors, 2006 *Rep. Prog. Phys.* **69** 327-396

7 **http://pubs.acs.org/cen/coverstory/83/8326electronics2.html**

8 S. Chowdhury, Pull-in voltage study of electrostatically actuated fixed-fixed beams using a VLSI on-chip interconnect capacitance, JMEMS. Vol. 15 No. 3 2006 639-651

9 J. Tsaur et al., Broadband MEMS shunt switches using PZT/Hf02 multilayered high k dielectrics for high switching isolation, Sensors and Actuators A 121 (2005) 275-281

10 J. Noel et al., Cryogenic pull down voltage of Microelectromechanical switches, JMEMS Vol. 17 **No**. 2, 2008 351-355

11 Yo-Tak Song et al., Low actuation voltage capacitive shunt RF MEMS switch having a corrugated bridge, IEICE Trans. Electron. Vol. E89-C No.12 2006 1880-1887

12 E. Yamashita, An approximate dispersion formula of microstrip lines for computer-aided design of microwave integrated circuits, IEE Trans. Micro. Theory and Tech. Vol. MTT-27 **No**. 12 1979 1036-1038

13 Z. J. Yao et. al, Micromachined low loss microwave switches, J. Micromech. Syst. Vol. **8** No. 2 1999 129-134

14 S. Kobayashi, A capacitive RF MEMS shunt switch, 2004, www.usl.chiba-u.ac.jp/~ken/Symp2004/PDF/D2.PDF

15 W. Hilbert, From approximations to exact relations for characteristic impedances, IEEE Trans. on Micro. Theory and Tech. Vol. MTT-17 **No**. 5 1969 259-265

16 H. Wheeler, Transmission line properties of parallel strips separated by dielectric sheet, IEEE Trans. on Micro. Theory and Tech. Vol. 13 **No**. 2 1965 172-185
17 Schneider, Microwave and millimeter wave hybrid integrated circuits, The Bell System Tech. Journal, July-August 1969 1703-1726
18 G. Kompa, Practical Microstrip Design 2005
19 M. Frankel et al., Terahertz attenuation and dispersion characteristics of coplanar transmission lines, IEEE Trans. on Micro. Theory and Tech. Vol. 39 **No**. 6 1991 910-915
20 T.Q. Deng, Accurate and simple closed-form formulas for coplanar waveguide synthesis, Electronics Letter, Vol. 31 **No**. 23, November 1995 2017-2019
21 Pozar, David. Microwave Engineering: Second Edition. 1997
22 K. D. Sudipto, N.R. Aluru, Full-Lagrangian schemes for dynamic analysis of electrostatic MEMS, J. Microelectromech. Syst. '04 Vol. **13** No. 5 737-756
23 J. H. Park et. al, Reconfigurable millimeter-wave filters using CPW-based periodic structures with novel multiple-contact MEMS switches, J. Micromech. Syst. Vol. **14** No. 3 2005 456-463
24 R. He, On-wafer monolithic encapsulation by surface micromachining with porous polysilicon shell, J. Micromech. Syst. Vol. **16** No. 2 2007 462- 472
25 A. Morris, S. Cunningham, Challenges and Solutions for Cost-effective RF-MEMS packaging, '07
26 M. Esashi. MEMS for practical application with attention to packaging, '06 IMPACT Vol. 18 Issue 20 1-4
27 C. H. Tsau et. Al, Characterization of wafer-level thermocompression bonds, J. Micromech. Syst. Vol. **13** No. 6 2004 963-971
28 T. R. Hsu, MEMS Packaging, IET 2004 1-272
29 R. Mason et. al, Development of reliability test guidelines for microelectromechanical systems in military applications, IEEE Sensors Conference 2007 53-57
30 www.three-fives.com, Collaborative work on MEMS packaging, September 2005
31 X. He et. al, Influence of wafer level packaging modes on RF performance of MEMS phase shifters, 2006 7th International Conference on Electronic Packaging Technology
32 J. Bouchaud et. al, Will RF MEMS live up their promise? Microwave Conference, 2006 1076-1079
33 A. Partridge et. al, The 9th SEMI Microsystem/MEMS Seminar, p. 55 2005.
34 R. Al-Dahleh et. al, Novel Warped-Beam Capacitive MEMS Switches, 2007 IEEE/MTT-S (Microwave Symposium) 1813-1816
35 Y. Kondoh et. al, High-Realibility, High-Performance RF Micromachined Switch Using Liquid Metal, J. Micromech. Syst. Vol. **14** No. 2 2005 214-220
36 A. Fargas-Marques et. al, Resonant pull-in condition in parallel plate electrostatic actuators, J. Microelectromech. Syst. '07 Vol. **16** No. 5 1044-1053
37 T. B. Xu, Design, modeling, fabrication and performances of bridge-type high performance electroactive polymer micromachined actuators, J. Micromech. Syst. Vol. **14** No. 3 2005 539-547
38 M. Daneshmand, Redundancy RF MEMS multiport switches and switch matrices, J. Micromech. Syst. Vol. **16** No. 2 2007 296-303

39 A. Witvrouw, CMOS-MEMS Integration: why, how and what?, ICCAD 2006 826-827
40 A. Franke, Polycrystalline silicon-germanium films for integrated Microsystems, J. Micromech. Syst. Vol. **12** No. 2 2003 160-170
41 S. Sedky, Optimal conditions for micromachining $Si_{1-x}Ge_x$ at $210^0C$, J. Micromech. Syst. Vol. **16** No. 3 2007 581-588
42 E. Flater et al, In situ wear studies of surface micromachined interfaces subject to controlled loading, Wear 260, 2006 580-593
43 D. Dickrell and M. Dugger, Silicon oil contamination and electrical contact resistance degradation of low-force gold contacts, JMEMS Vol. 16 **No**. 1, 2007 24-28
44 J. Sune et al., On the breakdown statistics of very thin SiO2 films, Thin solid films, 185, 1990 347-362
45 C. Goldsmith et. al, Lifetime characterization of capacitive RF MEMS switches, 2001 IEEE MTT-S Digest 227-230
46 Rebeiz, G.M., RF MEMS: Theory, Design, and Technology, Wiley-Interscience, 2002
47 R. Chan, Low-actuation voltage RF MEMS shunt switch with cold switching lifetime of seven billion cycles, JMEME Vol. **12** No. 5, 2003 713-719
48 E. Thielicke et al., A fast switching surface micromachined electrostatic relay, The 121h International Conference on Solid State Sensors, Actuators and Microsystems, Boston, June 8-12, 2003 899-902
49 G. Wang, et at., Novel reliable capacitive MEMS switches with photodefinable metal-oxide dielectrics, JMEMS Vol. 16 No. 3, 2007 550-555
50 S. Majumder, Study of contacts in an electrostatically actuated microswitch, IEEE 1998 127-132
51 Radant MEMS, Single Throw Single Throw Switch http://www.radantmems.com/radantmems.data/Library/Radant-Datasheet101_1.1.pdf
52 Radant MEMS, Single Throw Four Throw Switch http://www.radantmems.com/radantmems.data/Library/Radant-Datasheet240_1.1.pdf
53 Radant MEMS, Single Throw Single Six Throw Switch http://www.radantmems.com/radantmems.data/Library/Radant-Datasheet260_1.1.pdf
54 O. Rezvanian et al., Surface roughness, asperity contact and gold RF MEMS switch behavior, JMEMS Vol. **17** No. 3 2007 2006-2015
55 J. Lee, A pi small signal model of MEMS series switches based on the parameter extraction method, IEEE 2004, 502-508